Recent Developments in Nuclear Data for ADS

P. Talou[*], M.B. Chadwick[†], and P.G. Young[‡]

T-16, Nuclear Physics Group, Theoretical Division
Los Alamos National Laboratory, Los Alamos, NM 87545.

Lecture given at the:
Workshop on Nuclear Data for Science and Technology:
Accelerator Driven Waste Incineration
Trieste, 10-21 September 2001

LNS

[*]talou@lanl.gov
[†]mbchadwick@lanl.gov
[‡]pgy@lanl.gov

Abstract

Modern particle accelerators offer new opportunities to dramatically reshape the way we think about nuclear energy, and challenge some of the thorniest problems linked to its industrial use, e.g. nuclear waste. A powerful proton accelerator driving a sub-critical fission reactor could be used for producing energy more safely and burning up the extra spent fuel which so far has been stored in geological repositories. Although large R&D efforts are required to successfully implement such Accelerator Driven Systems (ADS), an important theoretical effort is also required to extend the nuclear data libraries, originally developed for existing nuclear reactors needs. The energies and isotopes involved in ADS do not necessarily overlap the range covered by the current nuclear reactors, and therefore there is a strong and urgent need to review and complement the nuclear cross sections databases to efficiently and safely build these ADS.

In this workshop, we will review some of the strength and deficiencies in the existing nuclear data libraries, for applications to ADS projects. A major step forward to extend these libraries has been achieved recently by the release of the LA150 cross section library [M.B. Chadwick et al., NSE **131**, 293 (1999)], evaluating reactions cross sections for different materials important for ADS, up to 150 MeV incident energies. We will devote a rather large fraction of theses lectures to present the latest developments in LA150. We will also present various numerical simulations performed in order to test and benchmark this new data library.

Such evaluations rely on nuclear reaction calculations performed with the GNASH code, and on available experimental data. We will therefore briefly review the physical models used in these calculations and present their importance in the GNASH code.

Another part in developing accurate nuclear data library consists in the *evaluation* of available experimental data, as an attempt to significantly reduce the systematic uncertainties which always affect experimental results. We will present the Bayesian inference scheme as a powerful tool to achieve this goal, and will illustrate this concept with the example of the evaluation of ^{239}Pu (n,f), recently assessed in the context of the ATW/AAA[1] program in Los Alamos.

Keywords: Hauser-Feshbach theory, Bayesian inference scheme, la150 library

PACS numbers: 24.10.-i, 25.40.-h

[1] Accelerator Transmutation of Waste / Advanced Accelerator Applications.

Contents

1 The Importance of Nuclear Data for ADS

Modern particle accelerators such as the ones developed in Los Alamos [1] and at CERN, Geneva [2] are capable of performances unthinkable even a decade ago. In Los Alamos, the proton linear accelerator delivers protons of 800 MeV with a few mA of current. The low-energy demonstration accelerator (LEDA) also built at Los Alamos National Laboratory can now deliver proton beams at the very high-intensity of 100mA. In Geneva, the CERN PS (Proton Synchrotron) accelerator is capable of delivering protons at an energy up to 28 GeV, with a flux of $2 - 3 \times 10^{13}$ protons per pulse. When hitting a heavy spallation target like lead, as many as 2×10^{16} neutrons are produced at each pulse. This extraordinary source of neutrons can then be used for different applications, ranging from very basic science to applied industrial use. All the applications which result from this spallation mechanism have been gathered under the appellation *Accelerator-Driven Systems* or *ADS*.

Neutron and proton induced reactions are ubiquous in the Universe and, more modestly, in our human activities. They participate largely to the so-called nucleosynthesis, i.e. the formation of the fundamental atoms in the Universe [3], through the s-, r- and p-processes. On the other hand, neutron induced fission reactions constitute the driving force in most human nuclear applications, e.g., production of energy in civil nuclear reactors or production of isotopes for medical applications [4]. Knowing precisely how neutrons and protons interact with matter is therefore of fundamental importance. We here step into the crucial field of *nuclear data evaluation* and *nuclear reaction modeling*. Since the heyday of nuclear physics in the 40-50's, important experimental and theoretical efforts have been devoted to the accurate determination of reaction cross sections[2] of some importance in the fields mentioned above. While the modern theoretical modelings of nuclear reactions provide an overall good picture of the physical processes involved, they still lack accuracy or predictive power in various specific applications. As of today, a clear understanding of the nucleon-nucleon forces extracted from basic physics principles is still noticeably lacking. Therefore, where the physical models fail to reproduce or predict experimental data, nuclear data libraries need to take over in order to allow applications to be developed or broader physical phenomena to be understood. Providing the overall nuclear physics community with accurate nuclear data libraries of various reactions cross sections therefore constitutes the cornerstone for many scientific and industrial activities.

The recent astonishing developments in particles accelerators technology opened up new areas of great scientific and industrial interest. For historical reasons, the existing nuclear data libraries have been primarily developed to encompass reactions cross sections of interest for the civil nuclear reactors design, for controlled thermonuclear fusion technologies, and of course for defense applications. Although the task is obviously overwhelming, progress in these areas has been prodigious. Unfortunately (or should we say- fortunately!) the new ADS require nuclear data beyond the standard regions of energy and isotopes studied so far.

We will devote the following sections to present some of these new applications, along with their requirements in terms of nuclear data libraries. In particular, we will present a list of isotopes and their reactions of interest for ADS. These libraries are being developed and improved thanks to both experimental and theoretical efforts. As an introduction to

[2] A cross section is simply a measure of the statistical probability for a given reaction to happen.

the next chapter, we will see how both aspects have to been studied in parallel in order to create accurate databases.

1.1 Accelerator-Driven Systems: A New Game

Thanks to the recent progress of particle accelerators technology, several ADS designs have emerged, either to produce energy in a safer way or/and to get rid of the recurrent and nagging problem of nuclear waste disposal. In this section, we will briefly go through some of the most promising current ADS projects and ideas.

In US, the APT program (Accelerator Production of Tritium) began in 1995 in order to sustain the US nuclear defense capabilities. Tritium, a radioactive isotope of hydrogen which boosts the explosive power of nuclear warheads, decays at the rate of 5.5% per year and must therefore be continuously replenished. So far, tritium is recovered from dismantled nuclear weapons, fulfilling the present stockpile requirements. Nevertheless, a shortage is likely to appear in the near future.

Tritium can be made by capturing neutrons in He-3 (helium gas). The necessary neutrons can be produced by spallation, (p,xn), in a linear accelerator like the one existing at Los Alamos. Current civil nuclear reactors can also be used for the same purpose. After a "dual-track" strategy period, the Department of Energy (DOE) finally opted for this second supply technology. Nevertheless, the APT program has been designated to act as a backup, if ever needed.

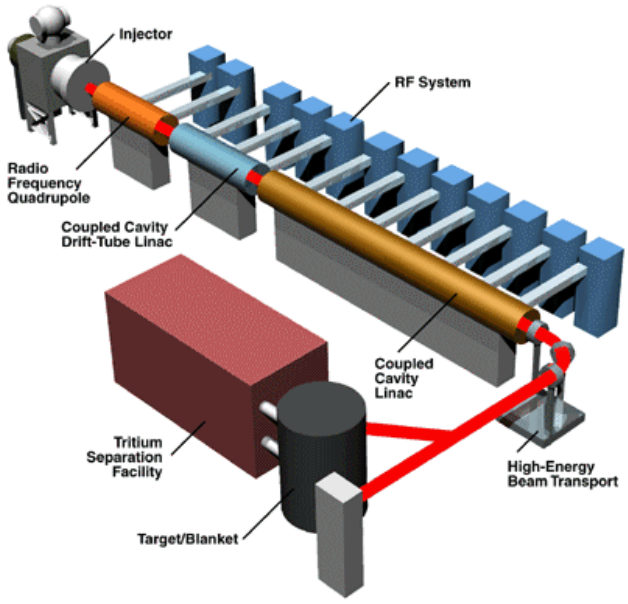

Figure 1: Linear accelerator used in the APT program at the Los Alamos Neutron Science Center (LANSCE), Los Alamos, USA.

The DOE decision was accompanied by incentives to develop an Accelerator Transmutation of Waste (ATW) program on the same basic principles used in APT [5]. This has led

to the proposed project of constructing an Accelerator-Driven Test Facility (ADTF), aimed at demonstrating the feasibility of nuclear waste transmutation technologies. This facility will also provide a test bed for advanced nuclear technologies and applications. The ADTF should be executed in less than 10 years.

Such a facility would also be used to produce significant amounts of the wide variety of medical isotopes that are required for the next generation of diagnostic and therapeutic nuclear medicine procedures [4]. Many of these isotopes are very difficult to produce with existing facilities, resulting in limited available quantities and high production costs. A facility such as the ADTF will be able to reduce these constraints significantly in providing large quantities of many of these isotopes at low cost.

Another ADS which has been getting a lot of attention in the last few years is the project of *Energy Amplifier* (EA) proposed by Carlo Rubbia[3] and his group, which aims at producing energy while burning the spent nuclear fuel at the same time [6]. Two versions could be developed: one optimized for the elimination of nuclear waste, a problem which concerns primarily the Western industrialized countries; another one optimized for energy production in developing countries where there is presently almost no nuclear waste.

In short, the EA is a subcritical fast neutron reactor, driven by a proton accelerator. A full description of the EA characteristics can be found in Ref. [7]. The protons are accelerated and used to bombard a very large target of lead to produce neutrons by spallation. These neutrons are then used to burn actinide elements coming from the nuclear waste stream generated by current nuclear reactors. Another essential characteristics of the EA is that ^{232}Th would be used instead of enriched ^{235}U usually used in PWR fuel. Thorium is an attractive fuel for several reasons: it exists in rather large quantities in the Earth's crust, it is isotopically pure, and is about 5 neutron captures away from the transuranic elements that we wish to destroy, making it more likely to be used in a transuranic destructive mode than a production one [6]. An EA could effectively destroy these elements through fission at about twice the rate at which they are produced in PWRs. Also, long-lived fission products (LLFP) such as ^{129}I and ^{99}Tc could be transmuted into stable elements in a parasitic mode around the EA, by using the adiabatic resonance crossing method [8]. While the radiotoxicity of these LLFP is rather small (less than the one observed from coal ashes!) after a few hundred years only, the fact that they are soluble in water and could therefore appear in the very long term in the biological chain "promote" them to the category of dangerous elements, akin to be destroyed.

In Europe, a roadmap [9] has been established and a plan to construct an ADS facility for transmutation of nuclear waste by the end of the decade is underway. Different concepts have been proposed, reflecting divergent nuclear policies on nuclear energy. For example, both France and Japan, countries poor in natural resources, consider plutonium as a very valuable resource for energy production. Therefore, the uranium fuel irradiated in light water reactors is reprocessed in order to extract the resulting plutonium, which is then reused with the uranium to fabricate mixed oxide fuel (MOX) for thermal reactors. On the other hand, countries like Sweden decided not to reprocess the plutonium. Hence, the transmutation processes could be slightly different according to the nuclear waste stream considered.

[3] Ex-director of CERN and 1984 Nobel Prize in Physics for the co-discovery of the W and Z^0 bosons.

Since the late 1970's, the Japan Atomic Energy Research Institute (JAERI) has been conducting research on an accelerator-driven subcritical system for the transmutation of long-lived radioactive nuclides [10]. The "OMEGA" program developed partitioning and transmutation technologies. Since 1998, JAERI and the High Energy Accelerator Research Organization (KEK) have been proposing the construction of an experimental ADS facility composed of a subcritical assembly and a liquid lead-bismuth target/coolant engineering facility.

Beside these mainstream programs, other ideas have emerged such as the thermal-spectrum molten-salt system proposed by D. Bowman [11]. However, we will not enter into further details here, and will let the interested reader access the broad literature on this subject.

1.2 Nuclear Data Libraries for ADS: Achievements and Remaining Problems

While divergences among nuclear energy policies appear worldwide, consequently affecting the precise design of an ADS for the incineration of nuclear waste, many components will be common to most ADS concepts, and very general nuclear data libraries can be developed confidently to encompass most existing problems.

In order to establish a list of isotopes important in a program of transmutation of waste, it is important to identify all possible sources for these elements. One obvious source is the production of waste from all civil nuclear reactors. Most common are the Pressured-Water Reactors (PWR) and Light-Water Reactors (LWR). These reactors produce some long-lived fission products (LLFP) along with actinides. As already stated above, ^{239}Pu is considered as a waste, and a proliferation problem, by US for instance, while in countries like France this plutonium isotope is recycled into MOX fuels and reinjected as a 30% component into the nuclear fuel for thermal reactors.

The higher actinides heavily produced in a PWR are gathered in Table 1.

PWR also produce significant quantities of Long-Lived Fission Products (LLFP), listed in Table 2. (n,γ) reactions allow to transmute these LLFP into stable or short lived nuclides. It is therefore crucial to know precisely their (n, γ) cross sections from the thermal region up to a few MeV.

The above mentioned elements constitute the bulk of waste which need to be destroyed or at least significantly reduced. A precise knowledge on the reactions cross sections used to transmute them is therefore crucial to obtain an efficient transmutation process. A recent report by the NEA/OECD agency describes the current status on minor actinide data [13]. Large discrepancies among various nuclear data libraries appear in places. V.N. Koscheev et al. [14] have performed several numerical simulations in order to test the accuracies of different nuclear data libraries for reactions on minor actinides and plutonium to predict results from integral and macroscopic experiments. Their findings are gathered in Table 3 where the achieved and required uncertainties for the most important reactions on minor actinides are estimated. Reducing uncertainties in these reaction cross sections can result in

Actinide	Half-life	ENDF/B-VI Quality on (n,f)
^{232}Pa	1.3d	None
^{237}Np	2.1×10^6y	Needs update
^{238}Np	2.1d	Reasonable
^{238}Pu	87.7y	Needs update
^{242}Pu	3.7×10^5y	Needs update
^{244}Pu	8×10^7y	Needs update
^{241}Am	432.7 y	Reasonable
^{242}Am	16.0h	Very Weak
^{242m}Am	141.0y	Needs update
^{243}Am	7.37×10^3y	Needs Update
^{242}Cm	162.9d	Very Weak
^{243}Cm	28.5y	Needs update
^{244}Cm	18.1y	Reasonable
^{245}Cm	8.5×10^3y	Needs update
^{246}Cm	4.73×10^3y	Needs Update
^{247}Cm	1.6×10^7y	Weak
^{248}Cm	3.4×10^5y	Needs Update

Table 1: Higher actinides produced in a PWR. The ENDF/B-VI quality refers to the estimates by P.G.Young et al. [12].

LLFP	Half-life	Production (per TWh_e)	LLFP/fission
^{79}Se	7×10^4y	20g	0.045%
^{93}Zr	1.5×10^6y	2.8kg	5%
^{99}Tc	2.1×10^5y	3.2kg	5.4%
^{107}Pd	6.5×10^6y	800g	1.2%
^{126}Sn	10^5y	80g	1.1%
^{129}I	1.6×10^7y	700g	0.9%
^{135}Cs	2×10^6y	1.4kg	0.17%
^{151}Sm	93y	60g	0.066%
^{90}Sr	28y	1.9kg	3.5%
^{137}Cs	30y	4.4kg	5.4%

Table 2: Long-Lived Fission Products (LLFP) production rate per Terawatt-hour-electric in a PWR reactor (source: Proposal for a n_TOF facility at CERN).

Nuclide	$\delta\sigma_c(\%)$	$\delta\sigma_f(\%)$	$\delta\sigma_{in}(\%)$
Np-237	15 (5)	7 (3)	30 (10)
Pu-238	25 (10)	10 (5)	40
Pu-239	6 (4)	5 (3)	20 (10)
Pu-240	10 (5)	5	20 (15)
Pu-241	15 (5)	5 (3)	20
Am-241	10 (5)	10 (5)	30 (10)
Am-242m	30 (10)	15 (5)	40
Am-243	30 (10)	10 (5)	30
Cm-242	50 (10)	15 (5)	30
Cm-243	50 (10)	15 (5)	30
Cm-244	30	10 (5)	30

Table 3: Actinide cross section uncertainties, achieved and required (in bracket), taken from V.N. Koscheev et al. [14].

significant improvements regarding the ADS overall safety (the neutron multiplier factor k_{eff} must stay below 1 for subcriticality) and the efficiency of the waste burning process. This could significantly reduced production costs and at the same time improve energy production as well as minor actinides and LLFP burn up.

Besides these obvious requirements for nuclear waste incineration, one also need to know the activation over time of the very constituents of an ADS transmuter. In general, an ADS is composed of a few elements, each exposed to a particular flux of particles. The materials in the target region are exposed to the direct proton beam and to secondary neutrons of spallation, ranging in energy from the primary beam energy down to thermal energies. During the irradiation of the ADS target, many elements are produced by spallation. Fortunately, most of them exhibit very short half-lives and do not influence the overall behaviour of the transmuter. However, a significant number of these products live much longer and could strongly influence the ADS over time. The materials surrounding the target area (salt fuel, blanket and moderator, coolants, and structural materials) are exposed to a very high flux of neutrons of spallation. Here is a list of these elements directly or indirectly exposed to the proton beam:

- Target materials: W, Pb, Bi, Th, U, Cr, Fe, Ni, Zr, Mo, Sn, He-3 (breeding material), + heavy water;
- Molten salt fuel carrier materials: Li, F, Be, Zr;
- Structural materials: C, Al, Si, P, Cr, Fe, Mn, Ni, Zr, Mo, Sn;
- Salt coolant: Na, B;
- Blanket/moderator materials: 1,2-H, Be, C, O

For all the spallation products and the subsequent decaying nuclei, one needs to know precisely all possible significant reaction cross sections (see Fig. 1 from Ref. [12]). The list of

materials requiring transmutation/activation/decay data is obviously quite extensive. Recently, very large data libraries on high-energy activation have been developed in Europe [15] and in Japan [10] to fulfill these requirements. In US, Chadwick and Koning have also developed similar large activation data files.

For all materials present in significant quantities in the target and surrounding region, neutron-induced data adequate for neutron transport calculations are required. These data are needed to calculate the energy distributions of down-scattered neutrons that drive the transmutation reactions in the blanket/moderator regions and, perhaps even more demanding, that can be used in shielding calculations for these complex, medium-energy neutron systems. Additionally, individual nuclide production or spallation yields are required, together with information on recoil nuclei energy distributions that can be used to obtain DPA and damage cross sections up to high energies for structural materials. Lastly, transmutation and activation cross sections are necessary for neutron-induced reactions, including cross sections for formation of isomeric states. In terms of nuclear reactions, the data required are neutron total, elastic and inelastic scattering, double differential (n,xn) and (n,xp), (n,γ), (n,f), (n,x), and (n,xγ) cross sections, plus production cross sections for individual nuclides as functions of Z and A with isomeric state production included.

For actual target materials, that is, materials that are exposed to the direct proton beam, essentially the same data requirements exist for proton-induced reactions as described above for neutron-induced reactions. Most importantly, (p,xn) and (p,xp) production cross sections are required as functions of incident energy and emission angle and energy for all materials directly exposed to the particle beam. Spallation product yields, recoil nuclei energy distributions, and (p,xγ) are needed, as well as information on isomer production. Proton-induced data would also be useful for materials that are not directly exposed to the proton beam, but these data are of lower priority than the incident neutron data.[end]

1.3 Improvement of Nuclear Data: Theory and Experiments

To improve nuclear data libraries, both experimental and theoretical efforts have to be developed. Where the predictive power of present nuclear reaction models is known to fail, at least at the accuracy required for given applications, new experiments are of primary importance. For instance, because of the relevance of actinide data, many projects for measurements of Am, Np and Cm isotopes are being developed under the auspices of the ISTC (International Science and Technology Center, Moscow). A recent European project, HINDAS [16], for High and Intermediate energy Nuclear Data for Accelerator-driven Systems, has started. Its main goal is to measure new reaction cross sections in the energy range between 20 MeV and 3 GeV on elements of crucial importance for ADS: Pb as a target element, U as an actinide, and Fe as a shielding element. A more general objective is to develop reliable modeling tools of nuclear reactions in 20-2000 MeV energy region.

This last point is important! While experiments obviously play a key role in our understanding of nuclear reactions, it would be quite impossible to perform as many experiments as are needed for any new application. It would be too costly and would also be counterproductive in the sense that a collection of data would be gathered without any attempt to

extract the fundamental underlying physics. Improving our nuclear reaction models from experimental knowledge is therefore of primary importance. It will increase our basic scientific knowledge, increase the predictive power of the physical models used, and extend their applicabilities.

Other large experimental programs include the already mentioned APT program at Los Alamos [1], which has already provided many data only partially analysed so far, and the n_TOF program at CERN [17] which aims at measuring neutron induced reactions for a large range of nuclides over a wide range of energies, from thermal up to 250 MeV. In the context of the APT program, large experimental data sets have been collected, in particular regarding the (n,total) and (n,f) cross sections for many isotopes of interest for ADS.

2 Nuclear Reaction Modeling

As this subject is treated in some details by other speakers of this workshop [18, 19], we will make this chapter brief in reminding the reader of the main physical models used for treating nuclear reactions, and in emphasizing on their implementations in the numerical code GNASH which has been used to perform the calculations described below.

2.1 Statistical Reaction Theory

Because of the tremendous complexity and of the significant number of degrees of freedom involved even in a simple nuclear reaction, its outcome can be predicted only in terms of probabilities, in the statistical sense. Several theories have emerged over the years to describe the full complexity of nuclear reactions over a wide range of incident energies. The first elementary neutron-induced reactions studied in the 1930's were sufficient for N. Bohr to invent the concept of compound nucleus (CN), of its formation and its decay [20]. Bohr's remarkable idea was that the collision between a high-speed neutron and a heavy nucleus will lead to the capture of the neutron by the heavy target, and the formation of a so-called compound nucleus, in perfect statistical equilibrium, where the incident energy of the neutron is equally shared among the nucleons of the target nucleus. Some time after this formation, and totally independent of it, the newly born CN will tend to emit radiations or particles to reach a more stable nuclear state. An essential feature of this decay process will be the competition between all the different open channels. The theoretical development of this genial idea came later with the Weisskopf-Ewing statistical theory of emission spectra [21], and then improved by Hauser and Feshbach who included the angular momentum and parity conservation law [22]. This enabled the calculation of reaction cross-sections to discrete states.

It was also early noted that some reactions like (d,p) occur without the formation and decay of a CN, but instead happen by direct transfer of a nucleon; this could easily be seen in the angular distributions of emitted particles forward peaked in the case of such *direct reaction* instead of distributions symmetric about 90° in the CN situation.

Obviously, these two reaction mechanisms describe two extreme situations, and early data

strongly suggested other, intermediary mechanisms where the incident nucleon plus target nucleus first go through a *preequilibrium phase*, during which particles can be emitted, before reaching the statistical equilibrium characterizing a CN stage.

In the following, we will briefly describe the models and theories associated with these ideas, as they are implemented in the GNASH code.

The Bohr independence hypothesis which states that the formation and the subsequent decay of a CN are two totally separate and independent processes, constitutes the basic idea behind the Hauser-Feshbach theory. How does this translate for the actual calculation of a reaction cross section? A simple mathematical formulation is

$$\sigma_{\alpha\beta} = \sigma_\alpha \times P_\beta, \tag{1}$$

where σ_α is the cross section of the formation of a compound nucleus in the channel α, and P_β the probability of seeing this system decay in the channel β. $\sigma_{\alpha\beta}$ is therefore the cross section of the reaction (α, β).

To fully describe a given nuclear reaction, a further assumption is made: a complex reaction process can be decomposed into a complicated chain (or tree) of binary reaction stages, as illustrated in Fig. 2. Each binary reaction stage must satisfy the following conservation laws of energy, spin and parity:

$$\begin{aligned} \epsilon + B_a = \epsilon' + E' + B'_a = U \quad & [\text{energy}] \\ \mathbf{i} + \mathbf{I} + \mathbf{l} = \mathbf{i}' + \mathbf{I}' + \mathbf{l}' = \mathbf{J} \quad & [\text{spin}] \\ p \times P \times (-1)^l = p' \times P' \times (-1)^{l'} = \Pi \quad & [\text{parity}] \end{aligned} \tag{2}$$

where ϵ and ϵ' are center of mass energies of incoming and outgoing particles a and a'; B_a and B'_a are binding energies of the particles relative to the compound system; i, I, p and P are spins and parities associated with light particles and the heavier target or residual nucleus; and l is the orbital angular momentum. The primed quantities indicate the outgoing channel.

The reaction cross section $\sigma_{a,a'}$ given by the statistical model reads

$$\sigma_{a,a'}\left(\epsilon, I, P; E', I', P'\right) = \sum_{J,\pi} \sigma_a(\epsilon, I, P; U, J, \pi) \frac{\Gamma_{a'}(U, J, \pi; E', I', P')}{\Gamma(U, J, \pi)}, \tag{3}$$

where (U, J, π) are the quantum numbers of the compound states through which the reactions proceed. The quantity $\Gamma(U, J, \pi)$ is the total decay width of the compound nucleus state (U, J, π) and is the sum of all possible decay widths,

$$\Gamma(U, J, \pi) = \sum_{a''} \sum_{E'', I'', P''} \Gamma_{a''}\left(U, J, \pi; E'', I'', P''\right), \tag{4}$$

where the summation over a'' includes all particles and gamma rays whose emission is energetically possible from (U, J, π), and the second summation includes all possible states (E'', I'', P'') in the various residual nuclei that result, consistent with the conservation laws given in Eq. 2.

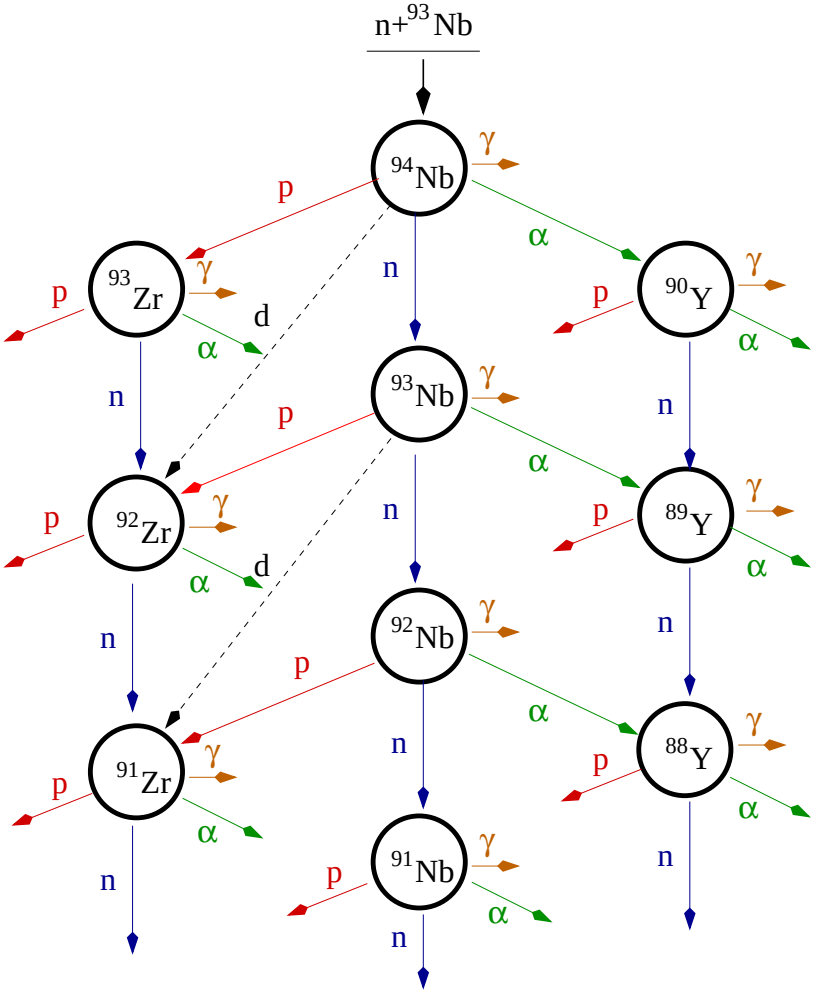

Figure 2: Reaction chain for calculations on neutron-induced reactions on ^{93}Nb.

The reaction cross section σ_a for formation of the compound nucleus can be expressed in terms of optical model (see explanations below) transmission coefficients, $T_{lj}^a(\epsilon)$, as follows[4]

$$\sigma_a(\epsilon) \propto \sum_{lj} f(l,\pi) \times T_{lj}^a(\epsilon) \tag{5}$$

where the function $f(l,\pi)$ is simply unity if the parity is conserved and zero otherwise, following the parity conservation law (see Eq. 2). Through the use of the reciprocity theorem which relates a cross section to its inverse (detailed balance), the decay widths can be related to the transmission coefficients:

$$\Gamma_{a'}(U,J,\pi;E',I',P') \propto \frac{1}{\rho(U,J,\pi)} \sum_{lj} f(l,\pi) T_{lj}^{a'}(U - E' - B_{a'}) \tag{6}$$

where $\rho(U,J,\pi)$ is the nuclear level density of the intermediate nucleus having the quantum numbers (U,J,π). While the above equations assume only discrete energy states, most GNASH calculations involve higher energy reactions where a continuum of states play a key role. Regarding these equations, it means augmenting all discrete summations with continuous integrals. GNASH analyses use the above relations to calculate in detail the populations of discrete and continuum levels for all spins and parities, for all nuclei involved in the chain reaction decay (see Fig. 2). We again refer the reader interested in the details of these calculations to the GNASH manual [23].

As stated above, the Hauser-Feshbach theory only describes the CN part of a given nuclear reaction. Direct processes like stripping or knock-out reactions can be treated externally to GNASH in a code like ECIS [24] which performs coupled-channel calculations. Preequilibrium processes are also usually treated apart, and used as a renormalization procedure after the Hauser-Feshbach calculations. We will come back in more details to these questions in the next paragraph.

2.2 The GNASH code

The GNASH code, developed in Los Alamos [23] and used largely around the World[5], simulates the chain of binary reactions predicted by the Hauser-Feshbach statistical theory, and calculates reaction cross sections and emission spectra for a wide range of reactions up to about 200 MeV[6] incident energies. GNASH computes preequilibrium and direct reactions as well. We will now describe briefly the different physical models which enter into an actual GNASH calculation. We will in particular emphasize on the most recent modifications useful for ADS calculations.

[4] For clarity purposes, we have intentionally removed most indices labelling the parameters used in the following equations. We refer the interested reader to the GNASH manual [23] for such details.

[5] It is worth noting that the GNASH code has been ranked very well in a recent international code intercomparison[26].

[6] This energy corresponds roughly to the pion production threshold, process which is not accounted for in GNASH.

2.2.1 Optical Models

The potential appearing in an optical model can be used to infer elastic, nonelastic, and total cross sections, along with the transmission coefficients $T_{lj}^{a}(\epsilon)$ needed for Hauser-Feshbach calculations. Indeed, the interaction of a projectile nucleon with a heavy target nucleus can be simulated in considering the nucleon moving in the single-particle potential create by the target nucleus. The asymptotic part of the nucleon wave function therefore determines the elastic scattering off the target nucleus. The imaginary part of the optical potential tends to damp the incident nucleon wave function in the elastic channel, and accounts for the total nonelastic part of the reaction. The optical model is of primary importance for any reliable reaction cross section calculation.

The T_{lj} coefficients are not calculated within GNASH but instead imported as an external input file. The transmission coefficients are obtained from either spherical or coupled-channels optical model calculations. Spherical calculations are usually performed with the nonrelativistic SCAT code by Bersillon [27]. For target nuclei which exhibit strong deformations (e.g., rare earths or actinides), coupled-channel optical model calculations are performed with the ECIS code [24] in order to obtain the transmission coefficients. Indeed, the deformation of the target nucleus mixes the different angular momentum components of the interaction, and all the different channels are therefore coupled and need to be treated in parallel. Note that the ECIS code is also used for spherical systems.

In some cases, specific nucleus-dependent potentials have been developed to fit as closely as possible the available experimental data. In other situations, a global nucleon potential like the one of Madland [25] is used.

Recent work in nuclear reaction theory has emphasized the importance of calculating direct inelastic scattering cross sections to low-lying states and indicated that collective direct excitations often persist into the continuum. For this reason, the GNASH code has been modified to allow the inclusion of direct scattering cross sections for large numbers of states (sometimes as many as 100), including those that are embedded within the "continuum" region, where a statistical level density prescription is used, such as excitation of giant resonances. For such direct reactions, nuclear deformation parameters are obtained from the literature, and the ECIS code is used to calculate the distorted wave Born approximation (DWBA) cross sections. These are then included as input to GNASH so that the effects of their subsequent gamma-ray decay, as well as the removal of flux from other reaction mechanisms, are incorporated into the results.

2.2.2 Level Densities

The Hauser-Feshbach calculations of reaction cross sections are very sensitive to nuclear level densities. While we generally have a partial knowledge on low-lying energy levels, and some clues on the overall shape of the continuum levels density, it is usually quite hard to infer intermediary energy states.

In GNASH, the continuum level density function $\rho(U, J, \pi)$, introduced in Eq. 6 above,

has the following form [28]:

$$\rho(U, J, \pi) = f(\pi) g(J, U) \rho(U), \tag{7}$$

where the spin and parity components are given by

$$f(\pi) = \frac{1}{2}, \tag{8}$$

and

$$g(J, U) = \frac{(2J+1)}{2\sigma(U)^2} exp\left[-(J+1/2)^2/2\sigma(U)^2\right]. \tag{9}$$

The quantity $\sigma(U)$ is a spin cut-off function given by the expression

$$\sigma(U)^2 \propto A^{2/3}\sqrt{aU}. \tag{10}$$

The energy-dependent level density $\rho(U)$ is usually calculated with the Gilbert and Cameron model [28], although the backshifted Fermi-gas model [29] has been used sometimes. More recently, the use of GNASH at higher incident energies has motivated the use of the Ignatyuk form of the Fermi-gas model [30]. This phenomenological model utilizes an energy-dependent level density parameter which allows to better fit experimental data, regarding in particular the effects of shell closures and of their washing-out with increasing energy.

2.2.3 Preequilibrium Emission

As a default, GNASH uses the *exciton model* to simulate the preequilibrium particle emissions. This simple model assumes that the nucleus formed by the reaction undergoes a series of particle-hole excitations stages, each allowing the emission of nucleons, before finally reaching equilibrium. The exciton model calculations involve solving a time-dependent master equation that describes the evolution of the system through a serie of two-body collisions, producing more and more complex configurations of particle-hole pairs. The master equation is simply

$$\frac{dP}{dt}(n,t) = \lambda^+(n-2)P(n-2,t) + \lambda^-(n+2)P(n+2,t) - \left[\lambda^+(n) + \lambda^-(n) + W(n)\right] P(n,t), \tag{11}$$

where

P(n,t) = probability that the excited nuclear system exists in the exciton state n (n≡p+h, the number of particles plus holes excited) at time t;

λ^+, λ^- = internal transition rates for n→n+2 and n→n-2, respectively;

W(n) = total particle emission rate from stage n summed over all outgoing particles and energies.

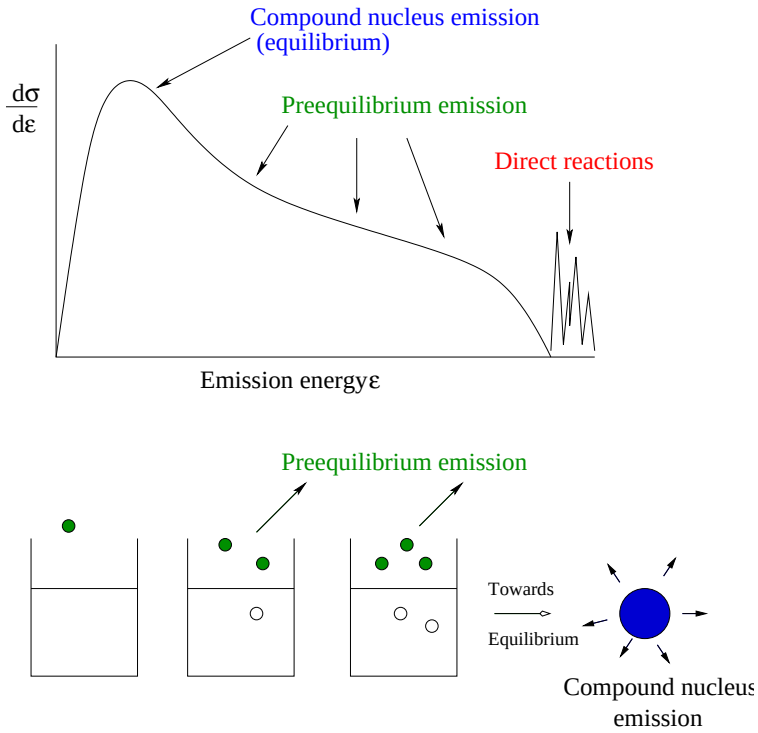

Figure 3: Schematic representation showing the compound nucleus, preequilibrium and direct reaction regions of a particle-emission spectrum, and the beginning of the preequilibrium reaction sequences that lead to equilibrium.

The actual physics appear in the calculation of the transition rates $\lambda^{\pm}$, but we will not enter into more explanations here (see [23] for more details). The initial condition of this equation is

$$P(p, h, 0) = \delta(p - p_0)\delta(h - h_0), \tag{12}$$

where the initial particle number is $p_0 = 2$ and initial hole number is $h_0 = 1$ for nucleon-induced reactions.

The exciton model in combination with the phenomenological Kalbach angular distribution systematics [31] provides a reliable method to predict double-differential outgoing spectra. The preequilibrium emission cross sections can also be calculated according to the quantum mechanical Feshbach-Kerman-Koonin (FKK) theory [32, 33]. The exciton model, more efficient in terms of computer execution time, has been benchmarked extensively against the FKK theory, which does not rely on experimental data for the prediction of angular distributions of outgoing particles. Therefore, extensive calculations like the ones performed in LA150 [38] have been done using the exciton model.

2.2.4 Recoil Spectra

The LA150 work includes the calculations of the energy spectra of secondary recoils, defined as all nuclides with $A > 4$. This addition to most previous works is important for the

detailed predictions of radiation damage and heating, and for simulations of heavy-particle radiotherapy [4].

In the 1960s, Blann and Ewart [34] exposed the basic physical principles governing recoil energies distributions. They made use of the Lindhard-Scharff-Schiott theory for the range-energy relationship. In short, in the formation of a compound nucleus, full momentum transfer from the projectile occurs. Compound nucleus evaporation of a particle leads to a new recoil that has, on average, a higher kinetic energy than the kinetic energy before emission. Where preequilibrium reactions occur in the first stages of the reaction, there is only a partial momentum transfer from the projectile, which results in lower kinetic energies of the first recoil nucleus after preequilibrium emission. Full details of our calculational method for recoils are described in Ref. [35]. Figure 4 illustrates some recoil spectra obtained in our calculations.

The initial composite nucleus lab velocity after the projectile strikes the target nucleus is rather large. However, since the first ejectile is often a preequilibrium emission with a large kinetic energy in a forward direction, the lab recoil speeds after this primary emission are reduced (which is another way of saying that only partial momentum transfer occurs). During further sequential compound nucleus decays, the recoiling nuclei tend to pick up speed again as internal excitation energy is converted to particle emission energy and recoil kinetic energy. An example of the variation in calculated recoil velocities with particle emission is shown in Fig. 5 for 80 MeV protons on ^{28}Si for processes involving sequential neutron emission. The initial reduction in recoil velocity due to first-particle preequilibrium emission is evident, followed by increasing average recoil velocity with sequential equilibrium neutron decay.

3 The LA150 library

The high-current proton accelerators currently designed for driving new applications involve protons of up to a few GeV incident energies. When hitting a heavy nucleus target, these high-energy protons create many spallation products, whom energy distribution can be as high as the incident protons energy. While intra-nuclear cascade codes work fairly well above, let's say 200 MeV, they are known to fail reproducing experimental data below this energy. On the other hand, nuclear reaction codes based on the Hauser-Feshbach statistical theory, like GNASH, do not generally handle pion production which occurs around 200 MeV. While such codes could be used to develop nuclear data libraries below 200 MeV, they have traditionally be used only below 20 MeV in the energy region important for fission and fusion reactors.

The development of new ADS has strongly encouraged the evaluation of nuclear data libraries above this artificial limit of 20 MeV. As part of this effort, Chadwick et al. [38] have developed new evaluated nuclear data libraries for incident protons and neutrons up to 150 MeV for a range of high-priority elements in the ENDF-6 format[7]. These new evaluated cross sections are collectively referred as the LA150 library.

[7]The Evaluated Nuclear Data Format (ENDF) is the format used in US for storing nuclear reaction evaluations; other formats exist worldwide (BROND- Russia, JEF- Europe, JENDL- Japan).

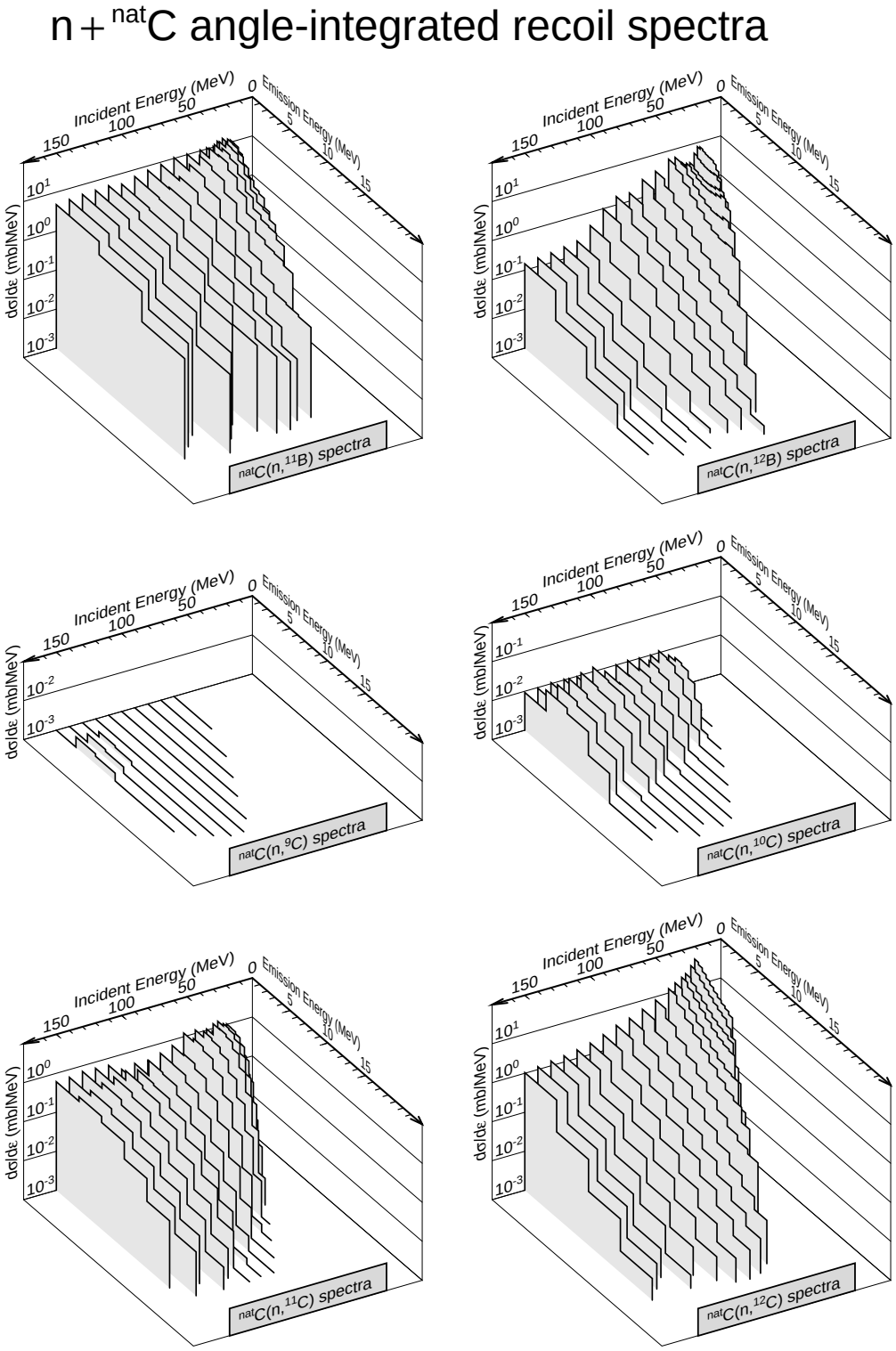

Figure 4: Three-dimensional graphical representations of recoil angle-integrated emission spectra from the ENDF evaluation for neutrons on carbon. The spectra are in the laboratory reference frame.

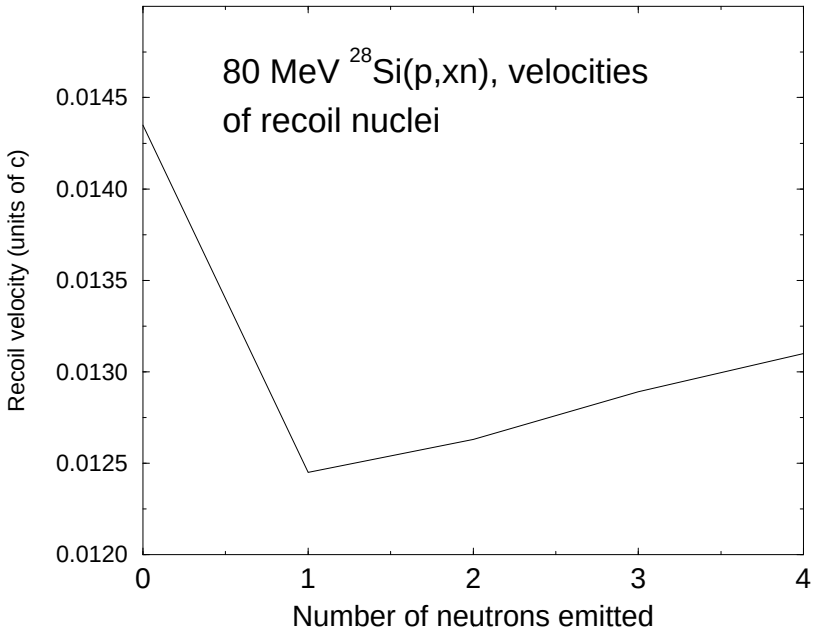

Figure 5: Variation in average velocity of recoiling nuclei as neutrons are emitted from decaying phosphorus isotopes in the 80 MeV $p + ^{28} Si$ reaction.

The choice of these high-priority elements has been dictated by the needs of the Accelerator Production of Tritium (APT) program which has been the primary source of support for this research (see Section 1.1). These elements are: H, C, N, O, Al, Si, P, Ca, Cr, Fe, Ni, Cu, Nb, W, and Pb, as well as Hg, owing to its importance as a spallation target for neutron-scattering material science studies. Most of these elements would also be of great importance for any accelerator-driven application; however, they do not include, for instance, actinides! Therefore, there is a strong need to extend these studies so they can be used for incineration of waste applications. The nuclear physics group, T-16, in Los Alamos is already planning such developments for the near future. However, the creation of high-energy data libraries for actinides is a challenging task because of the tremendous complications of multichance fission.

In the case of tritium production, the current design consists of a 1-GeV proton beam incident on a split tungsten target surrounded by a lead blanket. Through (p, xn) and (n, xn) nuclear reactions, neutrons are produced and are moderated by heavy water in the target region and light water in the blanket region. These moderated neutrons are subsequently captured on ^{3}He, which flows throughout the blanket system, to produce tritium via the (n, p) reaction.

In this work, nuclear model calculations have been used extensively to predict nuclear reaction cross sections for particle and gamma-ray emission because of the lack of measured data at higher energies. On the other hand, available measurements have constrained most of the evaluations for the total and total nonelastic cross sections. In any case, experimental data have been used extensively (where available) to guide and benchmark the present evaluations.

In the following pages, we will describe some of the LA150 results regarding isotopes

important for ADS. Throughout these results, we will try to adopt a pedagogical tone by illustrating concepts, methodology, problems that are usually encountered in this kind of work. Hence, the following results will only partially describe LA150, and we encourage the interested reader to wander on the T-16 Nuclear Information Service web page at `http://t2.lanl.gov/data/he.html` for more complete informations.

3.1 The $^{206-208}$Pb Evaluations

Lead plays a key role as a spallation target and neutron multiplier in many ADS designs, and therefore accurate nuclear data for lead isotopes are of crucial importance. Many measurements exist for the neutron-induced reactions on Pb. Figures 6, 7 and 8 represent the experimental data and evaluations for the total, elastic and nonelastic cross sections for lead.

In the case of the total cross section, we were guided mainly by the Lisowski et al. [36] and Finlay et al. [37] data. The elastic scattering angular distributions (Fig. 7) were calculated with a deformed optical potential developed for lead [41], and account for the experimental data very well. The total nonelastic cross section obtained from this coupled-channel calculation was modified slightly to better agree with the experimental data, as shown in Fig. 8.

The production cross sections of secondary ejectiles are simply the product of the nonelastic cross section by the ejectile multiplicity; it is therefore very important to obtain an accurate representation of the nonelastic cross sections to predict the chain of reactions happening in lead. Because of the small relative mass differences between lead isotopes, the evaluated total and nonelastic cross sections were assumed to be identical for all of them.

An optical model code like ECIS, in the DWBA mode, can be used to calculate direct inelastic scattering to low-lying levels in the target nucleus. This type of calculation has been performed in the lead isotopes, where both discrete and continuum regions were taken into account. Ninety-eight states were considered for ^{208}Pb up to an excitation energy of 7.114 MeV; in ^{207}Pb, 59 states up to E_x=6.483 MeV; and in ^{206}Pb, 13 states up to E_x=6.423 MeV. The Nuclear Data Sheets and Refs. [42] and [43] provided the deformation lengths used in the DWBA transitions.

The measurement by Hjort et al. [44] of the 65-MeV Pb (n,xn) reaction at forward angles is the only neutron-induced emission spectra measurement existing above 20 MeV. Such data are therefore extremely useful for benchmarking our neutron-induced GNASH calculations (see Fig. 9). The fall-off in the experimental data below 20 MeV is an artifact due to the high detector threshold energy. Some of the fluctuations seen in the measured data are due to the excitation of giant resonances high in the continuum not included in these calculations.

Numerous data for neutron production via Pb (p,xn) reactions exist. Figure 10 gathers the evaluated results and angle-integrated emission spectra measurements at 26, 45, and 80 MeV. The agreement is rather good at the two lowest incident energies; at 80 MeV, the calculations underpredict neutron emission in the 20-50 MeV region. This figure also illustrates the increasing importance of preequilibrium emission with incident energy, showing more high-energy ejectiles for the higher incident energy reactions.

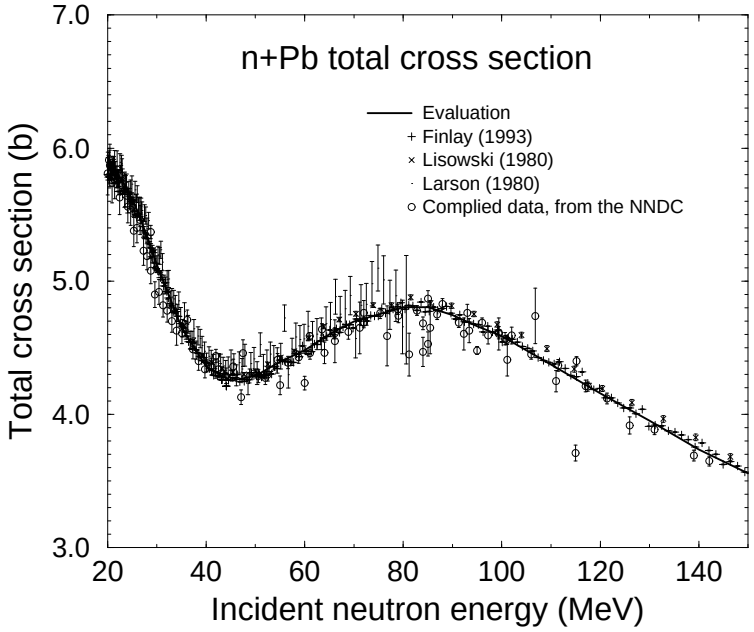

Figure 6: Evaluated neutron total cross section for ^{208}Pb compared with measurements.

At 113 MeV, the evaluation is compared to the doule-differential experimental data of Meier et al. [46] in Fig. 11. Agreement is fairly good over the whole emission energy for all angles but 150 deg. However, because of the small magnitude of the back-angle cross section, the practical impact of the disagreement should be negligible.

3.2 The ^{182,183,184,186}W Evaluations

The APT program uses tungsten as the spallation neutron target. Thanks to its high melting point, it can withstand large proton beam currents, and a very big number of neutrons are emitted per incident proton. However, tungsten exhibit a fairly high neutron capture cross section at low energies, therefore an split-target design has to be implemented to minimize neutron self-absorption.

The total cross section is expected to be very similar among the naturally occurring tungsten isotopes, and therefore our evaluation uses the same elemental cross section for all isotopes. The total n+W reaction cross section is shown in Fig. 12, as well as the p+W total nonelastic cross section. No measurement exist for the neutron nonelastic cross section on tungsten, though there is a 90 MeV measurement of the proton nonelastic cross section by Kirby and Link [48]. Therefore our evaluated nonelastic cross section makes a large use of optical model calculation results. When only very few data exist, it can be useful to look at reaction cross sections of neighbouring nuclei in order to guide the calculations. This is what has been done here: the data shown in Fig. 12 includes measurements on tantalum, adjacent to tungsten in the periodic table, which have been used to benchmark the optical model calculations.

The study of direct inelastic scattering reaction mechanisms in tungsten isotopes is very

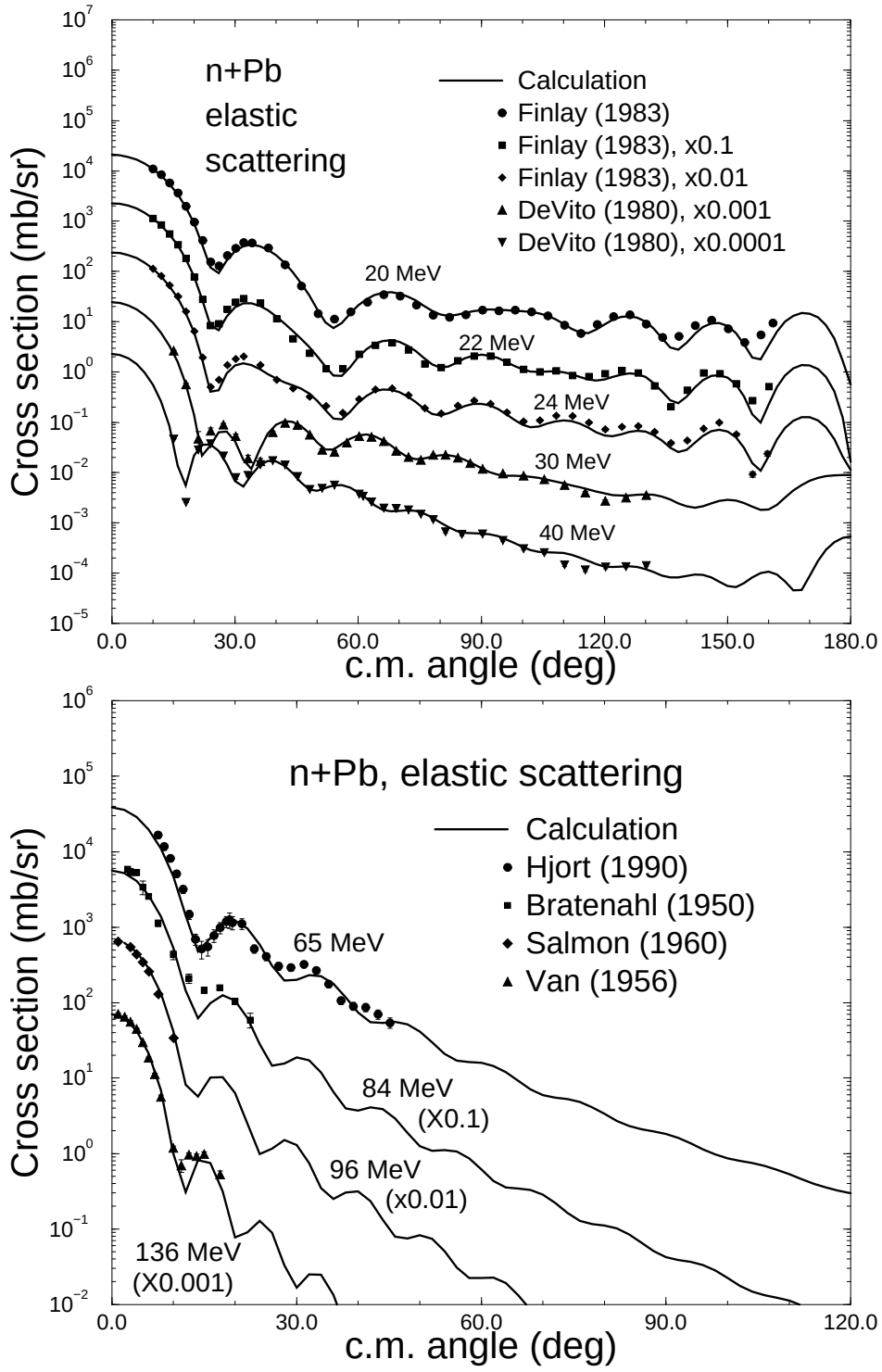

Figure 7: Evaluated neutron elastic scattering cross section for ^{208}Pb compared with measurements.

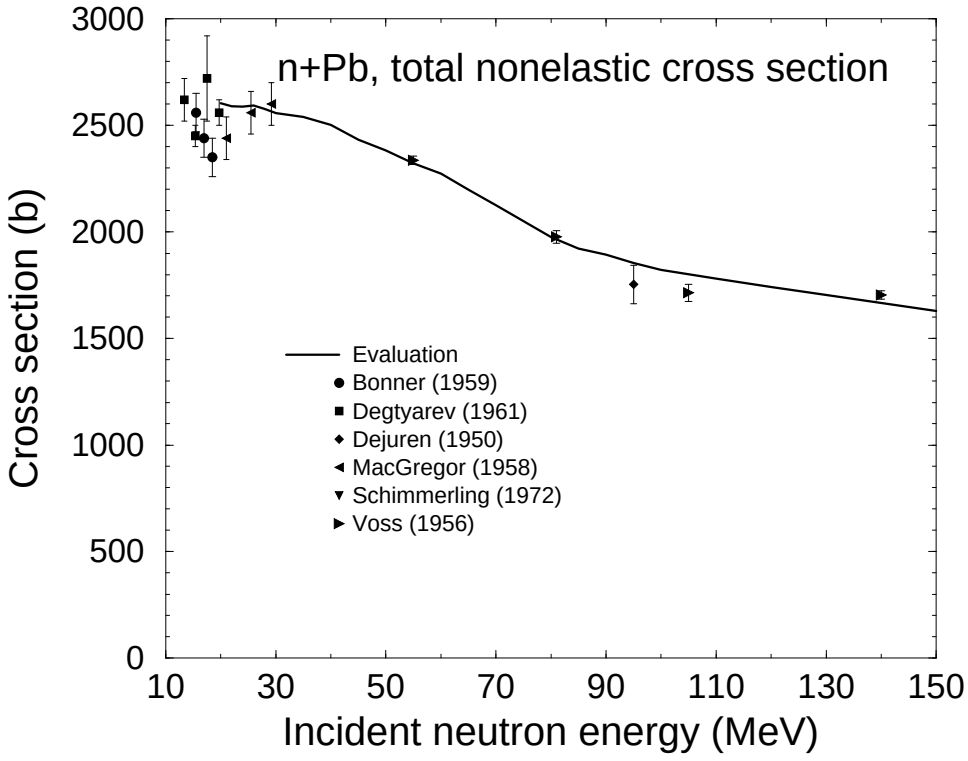

Figure 8: Evaluated neutron nonelastic cross section for ^{208}Pb compared with measurements.

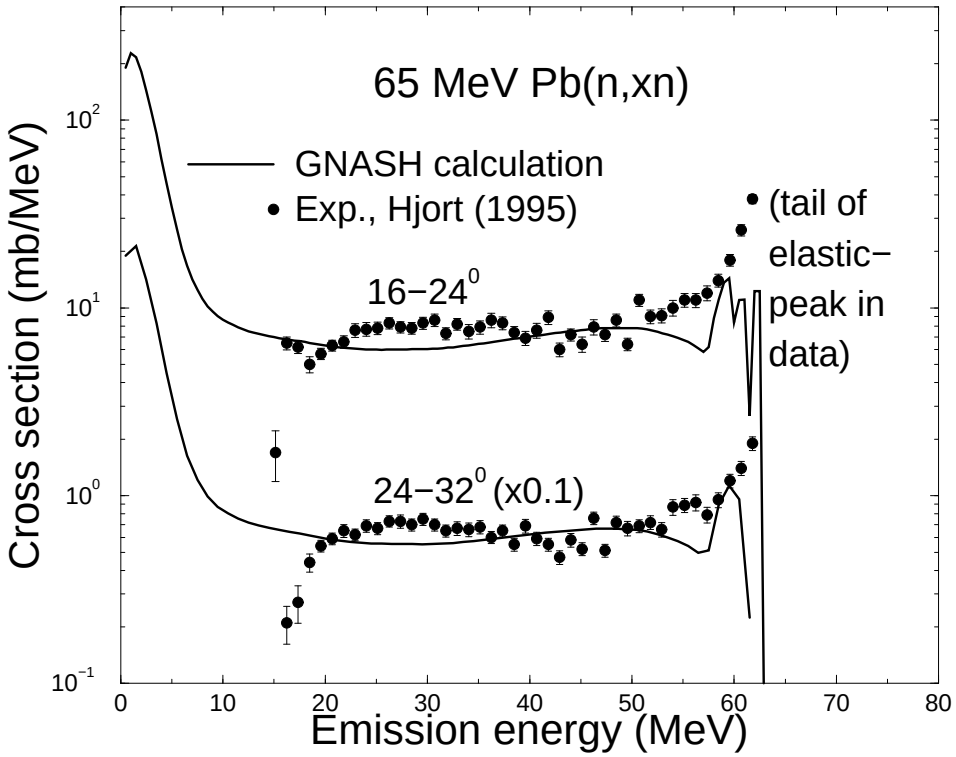

Figure 9: Evaluated ^{208}Pb (n,xn) neutron emission spectra t 65 MeV compared with experimental data [44]..

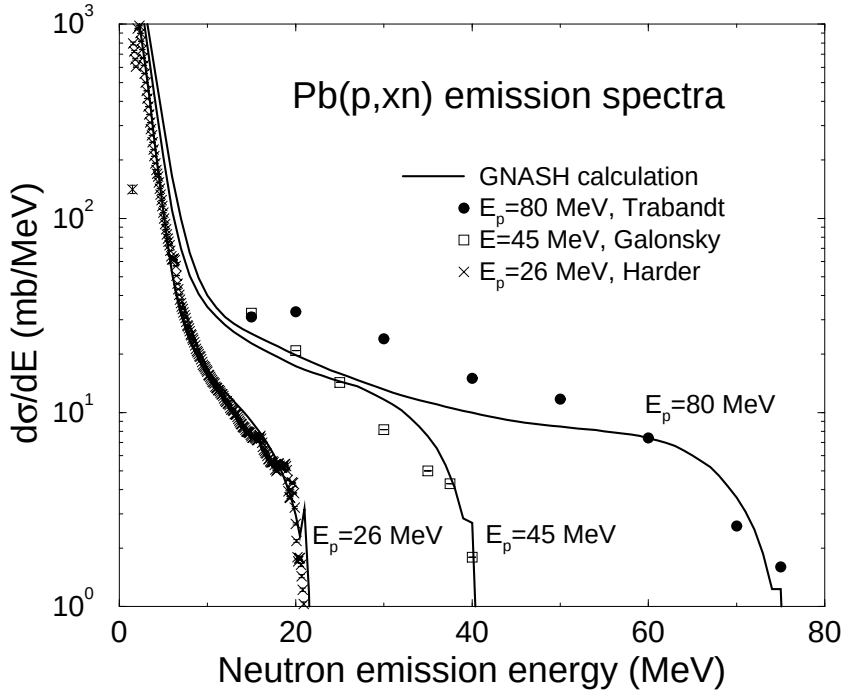

Figure 10: Evaluated ^{208}Pb (p,xn) angle-integrated neutron emission spectra compared with experimental data [45] at incident energies of 26, 45, and 80 MeV.

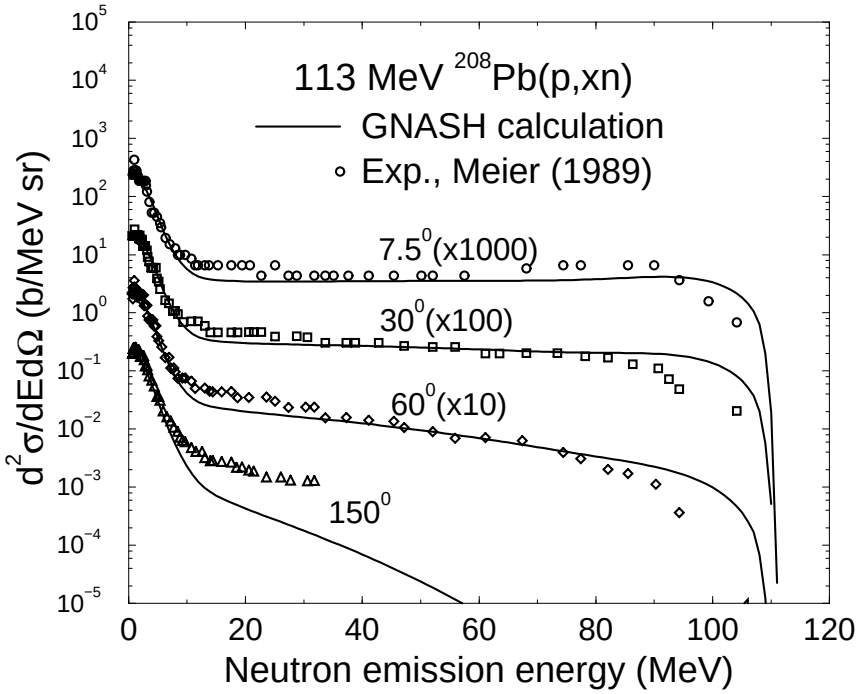

Figure 11: Evaluated ^{208}Pb (p,xn) double-differential neutron emission spectra compared with experimental data [46] at 113 MeV incident energy.

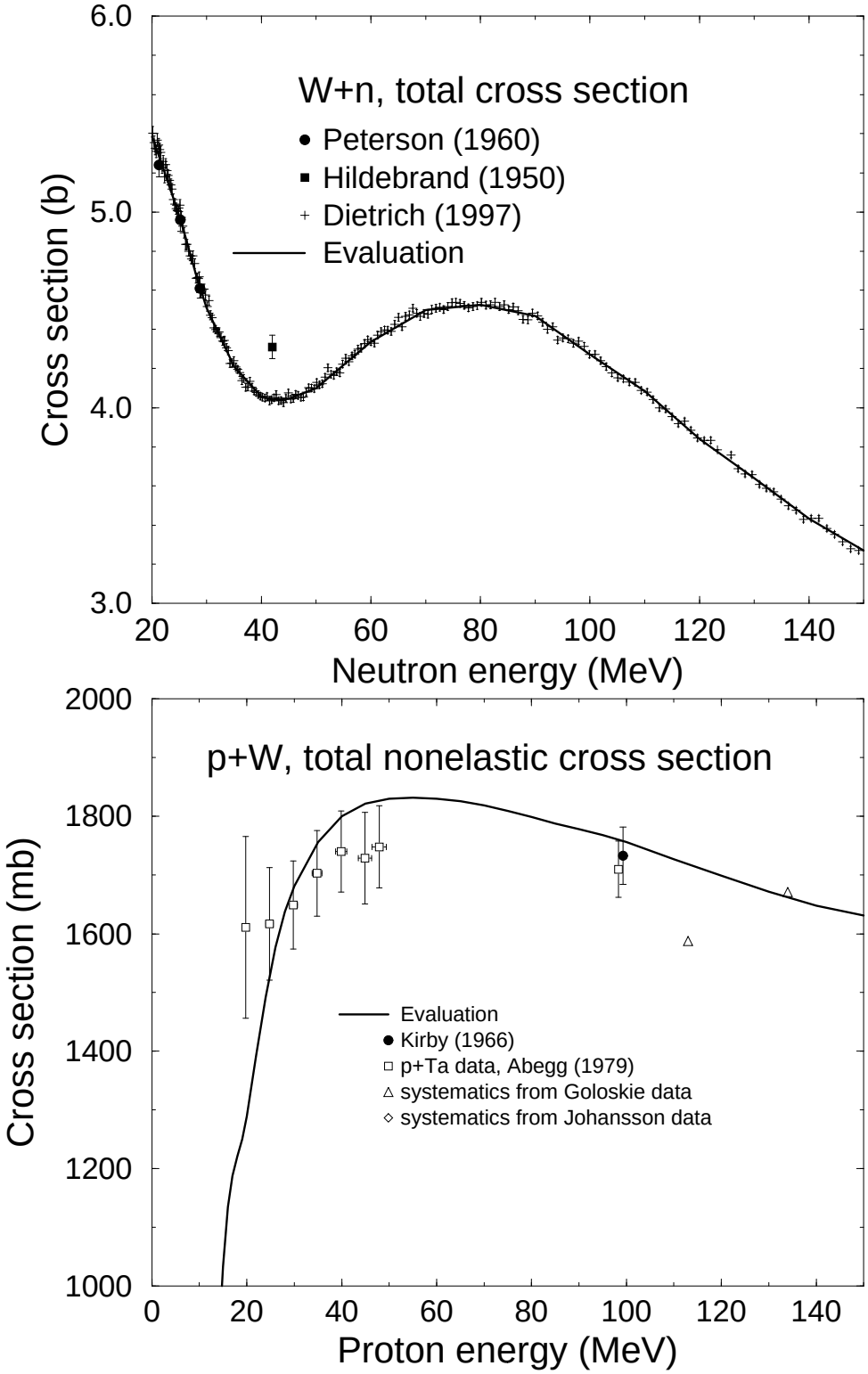

Figure 12: Comparison of tungsten evaluation and elemental measurements for (a) total neutron cross section [45, 47] and (b) proton nonelastic cross section.

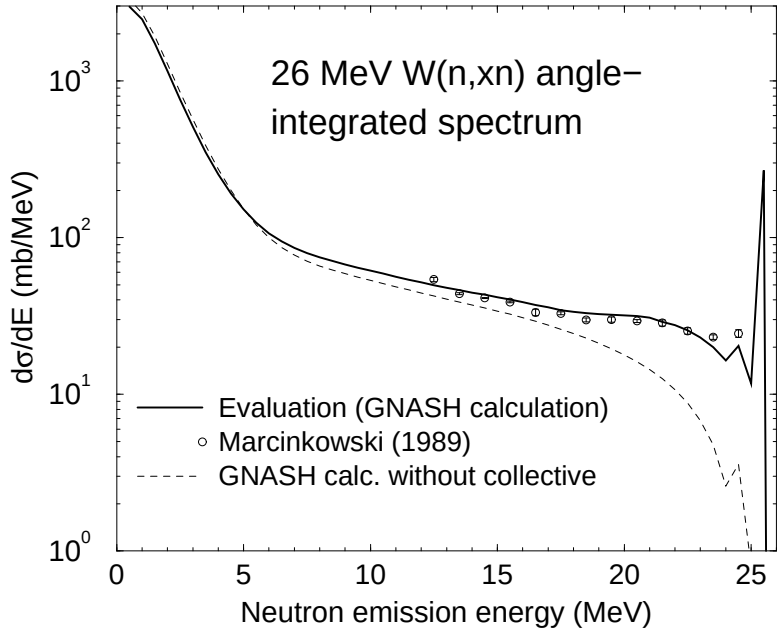

Figure 13: Comparison of the evaluated 26 MeV ^{184}W (n, xn) emission spectrum with measurements [49].

interesting, revealing the significant effect of collective excitations on some reaction cross sections. These scattering processes have been calculated with the ECIS code, and included (a) excitation of low-lying rotational levels and (b) excitation of giant isoscalar 1-, 2-, and 3- (low-energy octupole) resonances. Such resonances reveal the collective character of a nucleus, as compared to resonances fingerprinting direct reactions for instance, which involve only one nucleon amid many. The result of these calculations is plotted in Fig. 13 along with angle-integrated experimental data from Marcinkowski et al. [49]. The agreement is excellent. It is worth noting the significant contribution of the giant isoscalar broad resonances in the high-energy end of the spectrum (solid minus dashed curve).

3.3 The ^{58,60,61,62,64}Ni and ^{50,52,53,54}Cr Evaluations

Nickel and chromium are important structural elements in steel, and therefore appears naturally in any ADS design. Many experiments have been performed up to high energy incident nucleons ($\simeq$ 150 MeV). In particular, new data from Haight et al. [50] exist for neutron-induced alpha production up to $\simeq$ 50 MeV. Alpha emission can put stringent constraints on model calculations. Because it usually represents a very small fraction of the total reaction cross section, successfull nuclear model calculations are very sensitive to the level density and optical model parameters used. Alpha emission is therefore an important probe for the nuclear models used in our code.

Thanks to the numerous data available, the Ni neutron total cross sections were evaluated based on a Bayesian, least-squares method (see next section). The Ni isotopes cross sections were then transformed from those for natural Ni according to an $A^{2/3}$ dependence. These

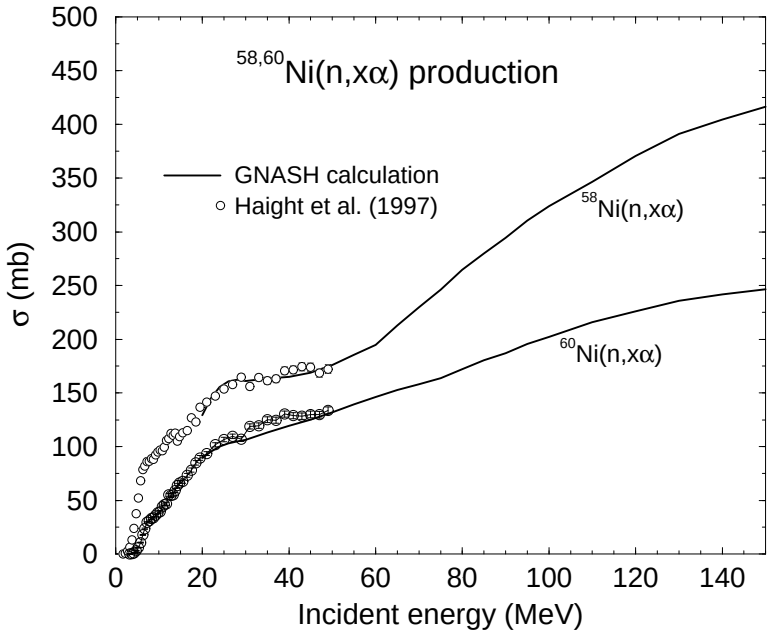

Figure 14: Alpha-particle production from Ni isotopes.

evaluated cross sections helped determine the optical model potential parameters for use in the ECIS code.

Figure 14 represents experimental data from Haight et al. [50] regarding the production of alpha-particles by neutrons incident on ^{58,60}Ni targets, along with the present evaluation where parameters have been carefully adjusted to account for the available experimental data (fine tuning of level density parameters).

In Fig. 15 are plotted experimental data on the production of protons, neutrons, deuterons and alphas from the 90 MeV ^{58}Ni (p, x) reaction [51, 52]. The calculations agree rather well with the data, except for the preequilibrium alpha emission at high energy which is overpredicted. It is worth noting that cross sections for cluster preequilibrium emission are very difficult to predict. One consolation though: the overprediction affects only the highest energy part of the spectrum where the production cross section is very low, hence the impact of this inaccuracy in an application should be small.

3.4 ^{54,56,57}Fe Evaluations and Radionuclides production

Iron is present in large quantities in the target/blanket region of an ADS. Its evaluation is therefore very important for nuclear transport calculations. Detailed calculations have been performed for the total, elastic, and reaction cross sections, and are described in Ref. [38]. Here, only a few points will be addressed.

Figure 16 shows secondary particle emission spectra following proton-induced reactions at different energies. The upper graph shows the calculated 113 MeV (p,xn) differential spectra at four angles, compared with the Meier et al. data [46]. Agreement is rather good, even at the backward angle, although the calculations overpredict neutron emission in the

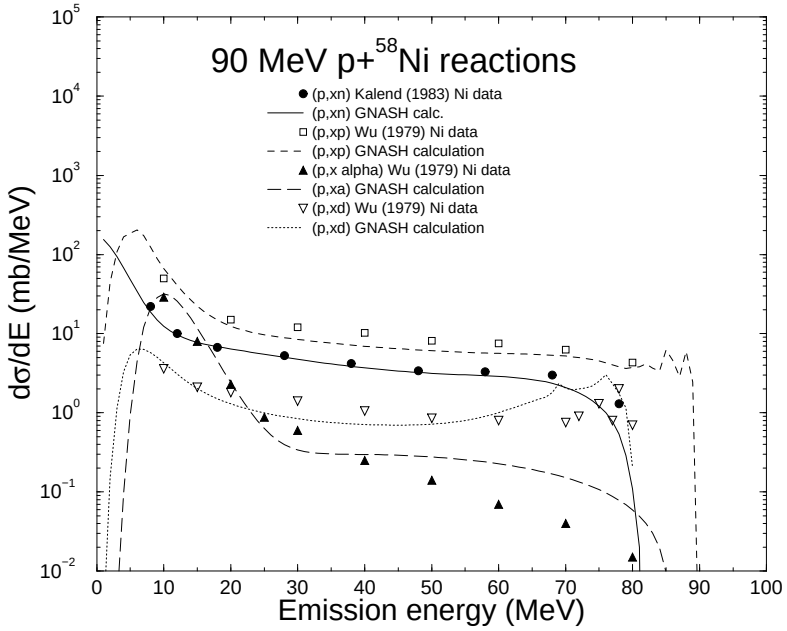

Figure 15: Comparison between calculated and measured [51, 52] angle-integrated emission of neutrons, protons, deuterons and alpha particles for 90 MeV incident protons on ^{58}Ni.

evaporation regime. At 60 MeV (Fig. 16b), (p,xp) experimental [53] and calculated angle-integrated spectra are compared successfully for ^{54}Fe. This figure also shows the emission spectra for ^{56}Fe, revealing the influence of the different Q values for the two isotopes; different Q values means that after particle emission, the respective residual nuclei are populated at different levels of excitation energy, where the level density is very different. Finally, the evaluated angle-integrated emission spectra at 22 MeV is compared with Svirin ^{56}Fe (p,xn) data [45]. The calculations underpredict the measured low-energy production by $\sim$ 20%.

As mentioned earlier, the LA150 evaluated library includes results for isotope production in order to facilitate studies of activation, energy deposition, and radiation damage. An example of such a result is shown in Figure 17 where the p+Fe isotopes production cross sections are plotted. It should be noted that the evaluation involved only ^{54}Fe and therefore does not fully correspond to the isotopic composition of natural iron. The agreement between evaluation and experiment is obviously best where the production cross sections are large (at the $\sim$20% level). However, the disagreement becomes significant for the smallest cross sections. These results are comparable to the best results shown in the recent international code comparison on intermediate energy activation yields [54].

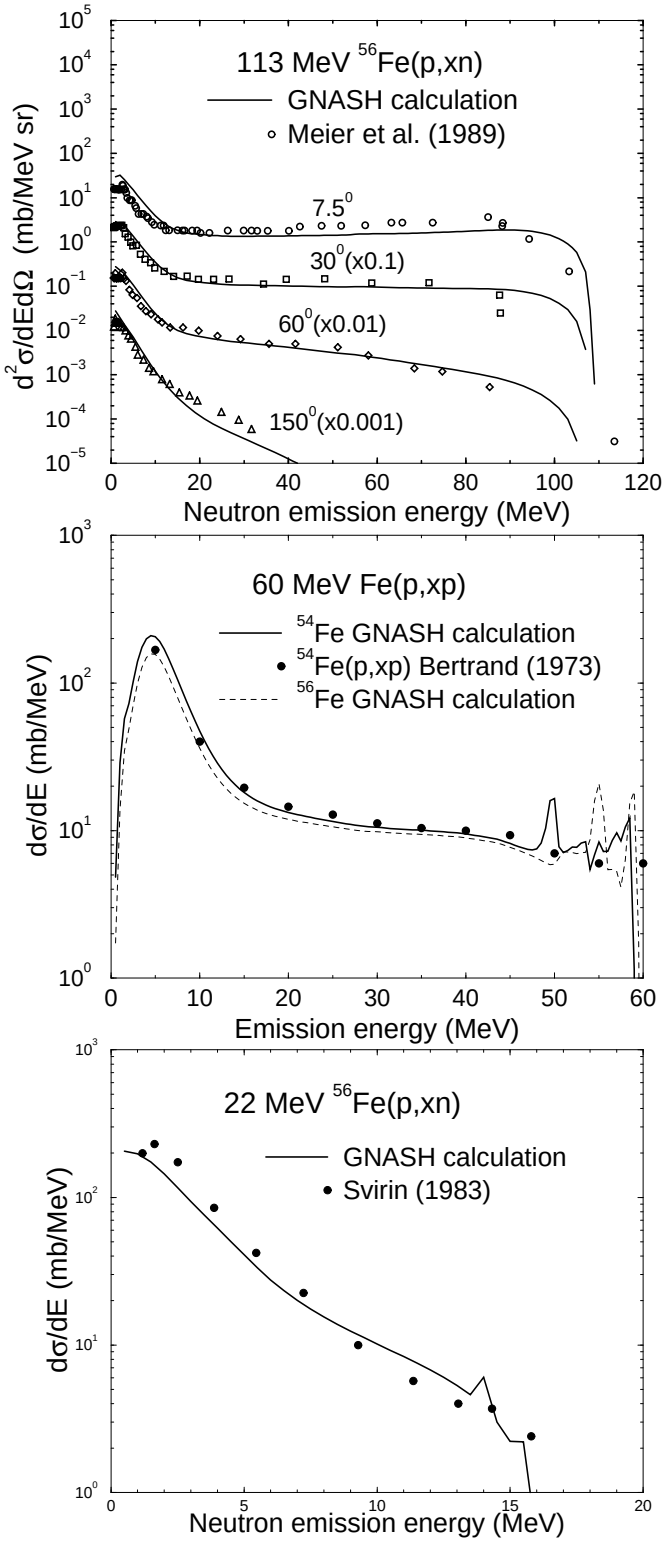

Figure 16: Comparison of evaluated p+Fe emission spectra with measurements.

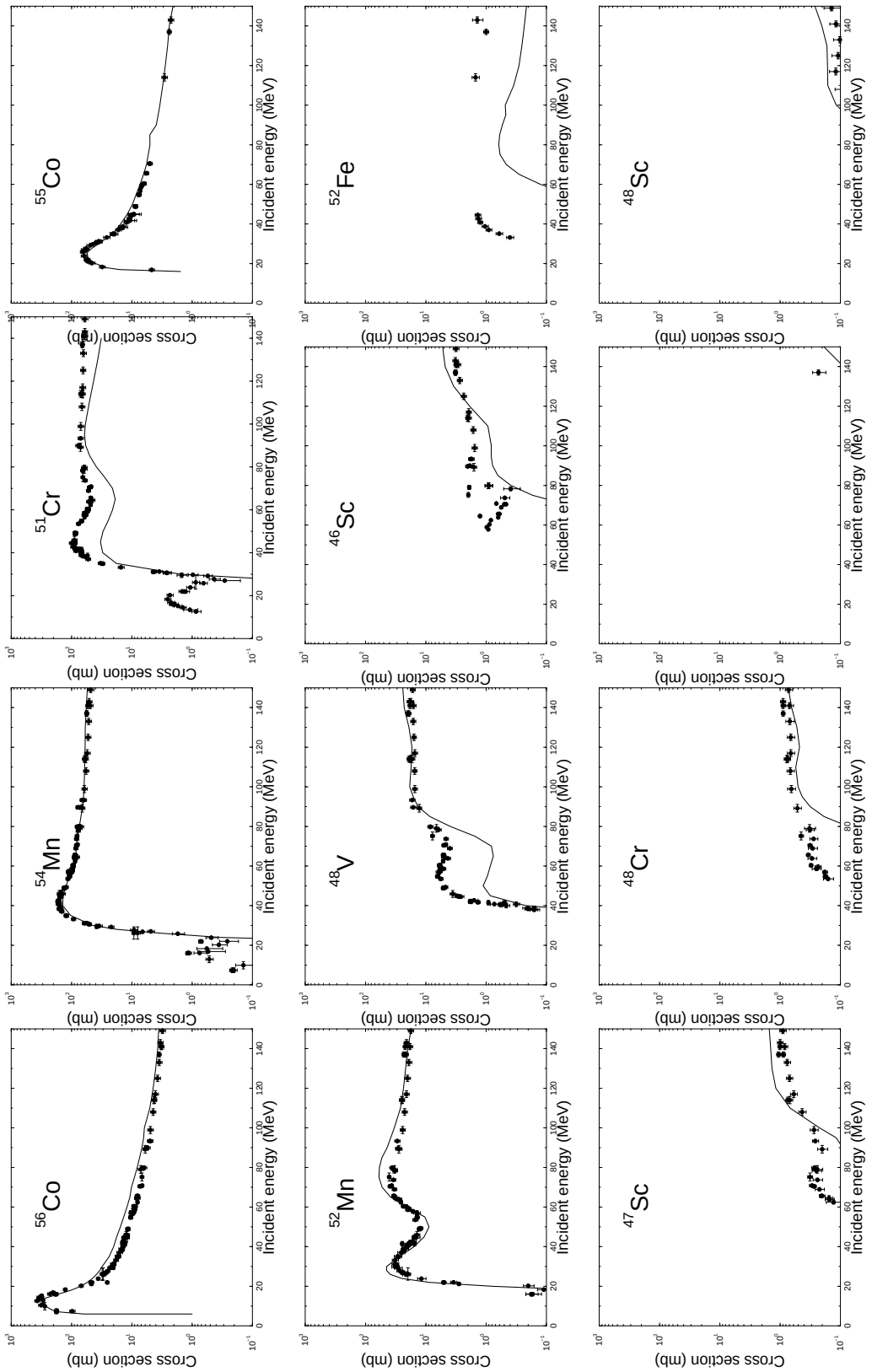

Figure 17: Comparison of evaluated $p + Fe$ radionuclide production cross sections with experimental data.

4 Benchmarking the LA150 Data in Particle Transport Codes

Various numerical simulations can be performed to test and benchmark the new LA150 data library. Below we will present some of the few tests that have been conducted against the LA150. More details can be found in Ref. [40]. Besides the development of high-energy data libraries, another major effort at Los Alamos has been the development of the Monte Carlo transport code MCNPX for high-energy applications. A recent status of the code and most of its features can be found in the review by Hughes et al. [55]. MCNPX has been used extensively to test the validity of the LA150 data.

4.1 n/p in spallation targets

A quantity of crucial importance in ADS designs is the total number of neutrons per proton (n/p) produced in a spallation target, since it governs both the overall economy and safety of the system. To test such a quantity, it is useful and practical to consider the following simple ideal model: a 1 GeV protons beam hits an infinite tungsten spallation target, and we calculate the number of thermalized neutrons finally produced per incident proton. Using MCNPX in the LAHET-physics mode, i.e., the intranuclear cascade model used at higher energies, or with the LA150 tungsten data, brings two significantly different results. In the first case, the n/p ratio obtained is 34.33 with a 1-sigma confidence interval of 0.14%. On the other hand, the result obtained with the LA150 data is n/p=33.17. To understand the origin of this difference, it is worth first noting that the neutron multiplication is governed by the so-called neutron yield, or multiplicity, which is given by the total neutron production cross section divided by the nonelastic cross section. The calculated values of the neutron yield from LA150 and LAHET-physics are shown in Fig. 18 (upper graph). The lower values for LA150 explains the lower n/p ratio found with GNASH- versus LAHET-physics. Why do we have such lower values? W (n,xn) neutron inelastic scattering data have been measured at 26 MeV incident energy (see Ref. [49]) and are plotted in Fig. 18 (lower graph), along with calculations using LA150 and LAHET-physics. The former calculations are in much better agreement with the data, and are considerably higher than the LAHET-physics results at higher emission energies. The reason that the LA150 library has a harder spectrum at the highest outgoing energies is that it includes a calculation of direct reaction processes where the neutron inelastically scatters off the nucleus, exciting giant-resonances and rotational collective states.

4.2 Proton-induced thick target neutron production

In order to predict accurately the behaviour of an ADS, nuclear transport codes ought to describe secondary neutron production very reliably. These neutrons are produced when the high-energy incoming protons interact with the target, blanket, and shielding materials of the ADS. Therefore, thick-target neutron production measurements constitute a wonderful testing ground for microscopic nuclear data libraries like LA150 associated with charged-particle

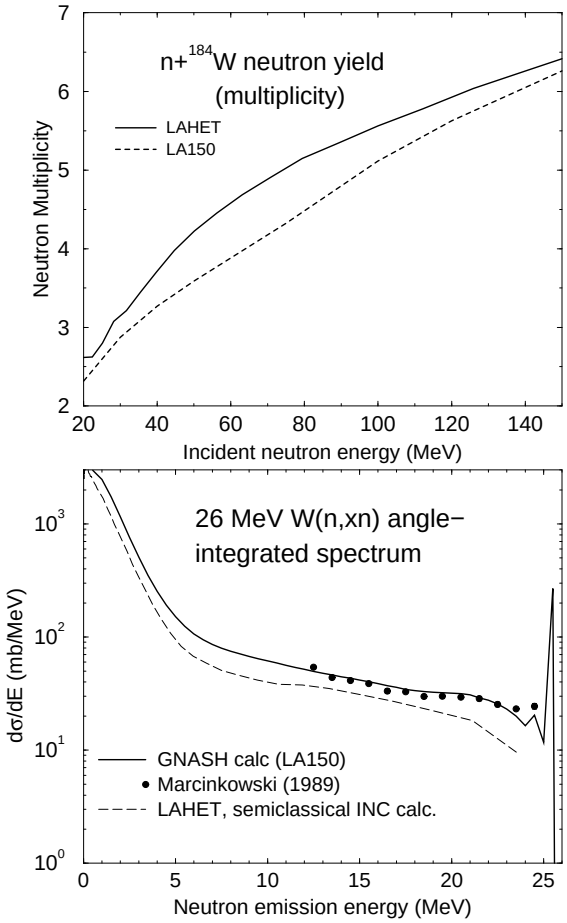

Figure 18: *Upper graph:* Neutron emission multiplicity for neutrons incident on tungsten, calculated by GNASH and by LAHET; *Lower graph:* Angle-integrated spectrum of neutrons following 26 MeV neutrons bombardment on tungsten [49], compared with GNASH and LAHET calculations.

transport algorithms implemented into MCNPX. The targets used in such measurements are usually thick enough to stop the incident protons completely, but "thin" enough- because of the absence of the Coulomb barrier, for secondary neutrons produced to escape without any additional interaction. Contrarily, the protons slow down from their maximum energy, while having for each energy a non-zero probability of producing secondary neutrons. Thick-target measurements therefore represent an integral over all incident energies up to the maximum of the differential "thin-target" cross sections, weighted by the stopping power function which quantifies how fast the particles slow down in the material.

Figure 19 shows experimental data [56] and MCNPX calculations, using LAHET-physics (dashed lines) and LA150 data (solid lines), for thick-target neutron production spectra from 30 MeV protons. The MCNPX results using the library data obviously perform much better than their LAHET counterparts. This result was expected since at low energies the semiclassical physics used in LAHET is known to fail. At higher energies, the quality of the two calculations tend to become similar (see Ref. [40] for more details).

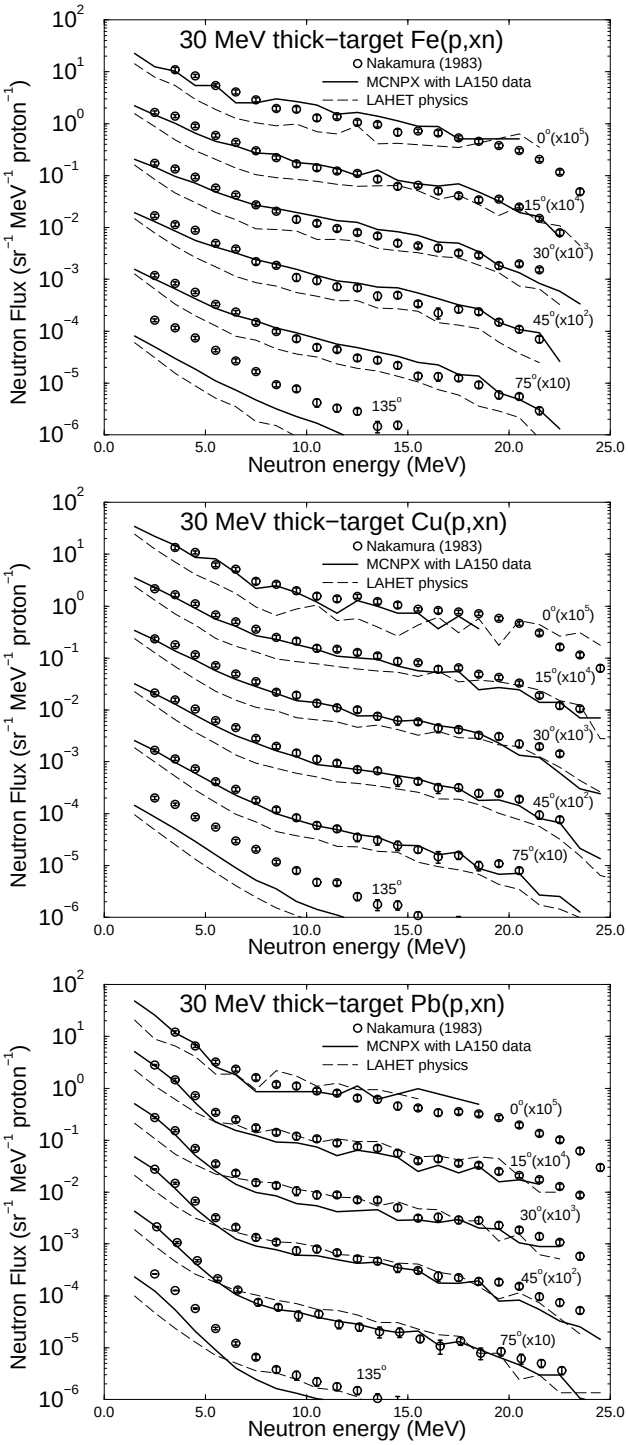

Figure 19: Thick target neutron production spectra for 30 MeV protons incident on Fe, Cu, and Pb [56] compared with calculations. The solid lines show MCNPX using the LA150 data, the dashed lines show MCNPX using LAHET physics.

4.3 Radiation damage

The NJOY Nuclear Data Processing System has been used to calculate the neutron damage energy cross section[8]. This cross section is used to calculate lattice defect production rates in materials, which are an important measure of radiation damage. The LA150 library is the first Los Alamos release of a continuous-energy MCNPX library to include the damage energy cross section. This addition is very important for accelerator applications, because of the severe radiation damage effects observed in accelerator-driven neutron sources.

Generally, at energies above 20 MeV, the LAHET code has been used for calculating this cross section. However, LAHET-physics, i.e., intranuclear cascade models, are known to be less reliable at energies below approximately 150 MeV, and substantial discrepancies between the predictions of LAHET and of data evaluations for the damage energy cross section have been noted at the transition energy of 20 MeV. The LA150 Library helps reduce these discrepancies by increasing the transition energy up to 150 MeV.

The damage energy cross section from the LA150 library is plotted in Figure 20 over the energy range 400 keV to 150 MeV for ^{12}C, ^{27}Al, ^{56}Fe, and ^{208}Pb. Also plotted is the damage energy cross section as calculated using LAHET over the energy range 16 MeV to 3.1 GeV.

4.4 Other applications

The LA150 has been tested and benchmarked through other applications like neutron transmission and shielding design, and neutron heating and kerma, very useful in medical physics for calculations of absorded dose in fast neutron and proton radiotherapy [58]. For details, we refer the reader to the article by Chadwick et al. in Ref. [40].

[8] A description of the theory of damage energy and the computation of damage energy are described in the NJOY Manual, Chapter 4 [57].

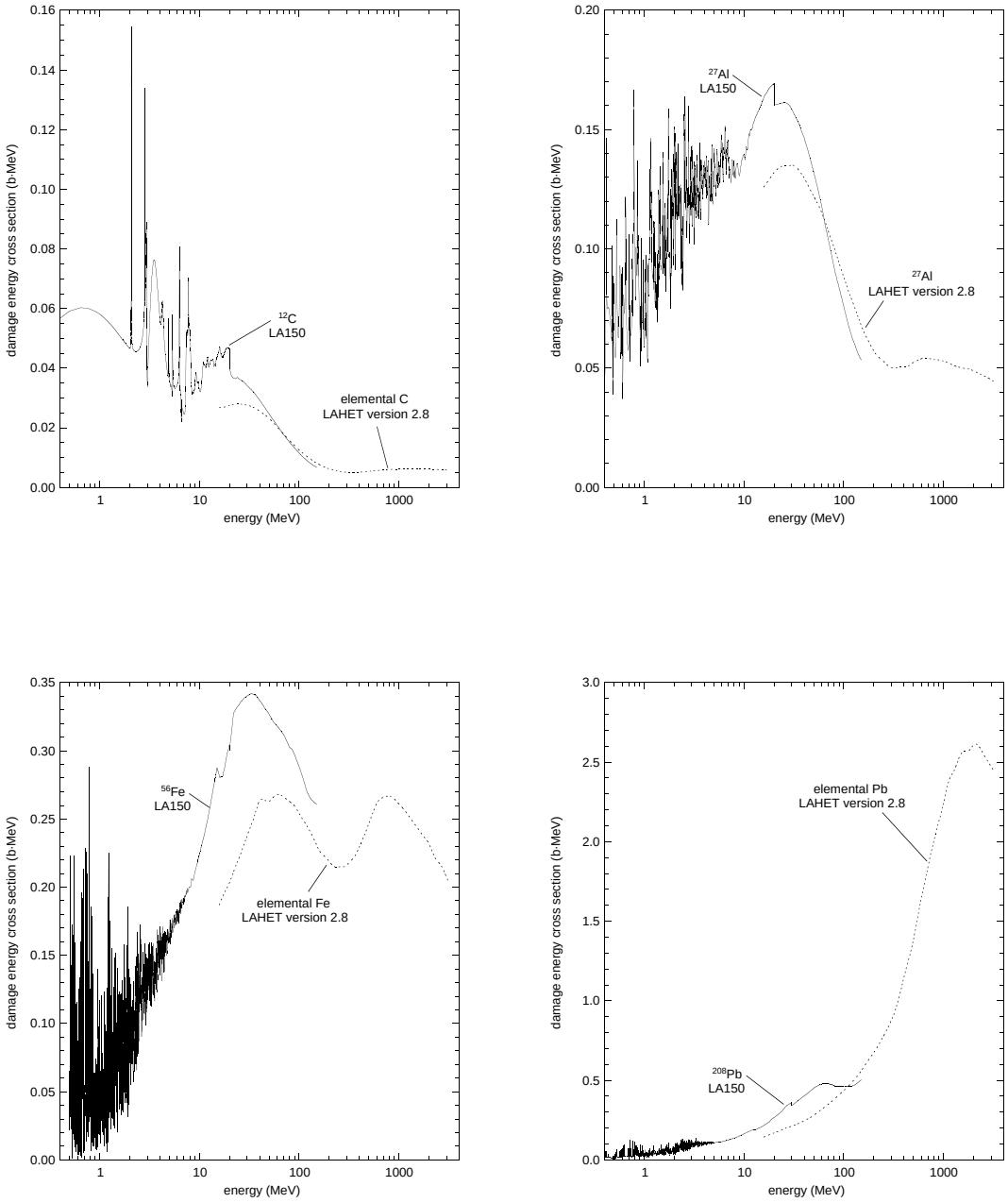

Figure 20: Neutron damage energy cross section from the LA150 library over the energy range 400 keV to 150 MeV for ^{12}C, ^{27}Al, ^{56}Fe, and ^{208}Pb. Also plotted is the damage energy cross section as calculated using LAHET version 2.8 over the energy range 16 MeV to 3.1 GeV.

5 Nuclear Data Evaluation: the Bayesian Inference Scheme

So far, we have presented nuclear reaction modeling techniques, the physical models used, and some results particularly interesting for ADS applications. The goal of such calculations and model improvements is of course to get a better description of physical phenomena and of their implications on specific physical quantities.

Another aspect of the development of data libraries deals with the so-called "data evaluation" process, and will be the subject of the next few pages. In short, data evaluation aims at finding the best estimate of a physical quantity or to establish which theory describes a particular phenomenon better, through a statistical analysis of a set of experimental data.

Let us start by quoting the great mathematician Henri Poincaré [59] to introduce the subject:

"I play at ecarté with a gentleman whom I know to be perfectly honest. What is the chance that he turns up the king? It is 1/8. This is a problem of the probability of effects. I play with a gentleman whom I do not know. He has dealt ten times, and he has turned the king up six times. What is the chance that he is a sharper? This is a problem of the probability of causes. It may be said that it is the essential problem of the experimental method."

Indeed, the experimental method tries in the end to answer some fundamental questions about the causes of a particular physical phenomenon. Of course, experimental data are usually affected by a certain degree of uncertainty. Experimental uncertainties have traditionally been classified into two separate categories: *statistical*, i.e., caused by variations in the results of repeated observations under (apparently) identical conditions; and *systematic*, i.e., inherent to a particular experimental setup. The first ones can therefore be reduced, in principle indefinitely, by repeating the same experience a large number of times. The second ones can only be modified by performing new, different observations.

Because of these uncertainties, an adequate theory can only be enounced in terms of probabilities. Obviously, the more experience we have, the more knowledge we gain; the process of learning from empirical observations is called *induction* or *inference* by philosophers. Since the 17th century, mathematicians and statisticians have worked on developing a mathematical and logical framework for such an inference scheme. Bayes' theorem constitutes the cornerstone for such mathematical tools.

In the following, we will briefly introduce the most important points in Bayesian inference methodology, and see how it can be used in the framework of the development of nuclear data libraries. We will terminate this section by providing the example of Bayesian approach to the evaluation of neutron-induced fission reaction on ^{239}Pu, an isotope of great importance for ATW program.

5.1 Mathematical Framework

The English clergyman Thomas Bayes (see Fig. 21) gave his name to a now famous theorem, published posthumously in a short memoir in 1763, which provides a convenient and logical

Figure 21: Reverend Thomas Bayes 1702-1761.

rule for updating the belief in an hypothesis against new evidence. Bayes' theorem is a direct consequence of the basic axioms of probability theory. The belief in a given hypothesis $\mathcal{H}$, after acquiring new knowledge D, and under some circumstances C reads

$$P(\mathcal{H}|D,C) = \frac{P(D|\mathcal{H},C)P(\mathcal{H}|C)}{P(D|C)}, \tag{13}$$

The left-hand term $P(\mathcal{H}|D,C)$ is called the *posterior*, and represents the new belief in the hypothesis $\mathcal{H}$ after gaining the new knowledge D. The term $P(\mathcal{H}|C)$ is the *prior* probability of $\mathcal{H}$ given C alone. Finally, the term $P(D|\mathcal{H},C)$ is the *likelihood* function which gives the probability of observing D if the hypothesis $\mathcal{H}$ and the circumstances C were actually true. The denominator $P(D|C)$ is independent of $\mathcal{H}$ and can be regarded as a normalizing constant. In other words, the Bayes' rule simply states

$$\text{Posterior} \propto \text{Likelihood} \times \text{Prior} \tag{14}$$

Naturally, such a rule can be applied iteratively each time new information becomes available. The mathematical tool of a *covariance matrix* allows one to take into account the eventual correlations between different set of informations.

There has been quite a lot of discussion and controversy on Bayesian inference scheme, and in particular to the 'subjectivity' in choosing priors. Indeed, the application of the Bayesian rule of updating knowledge assumes that we have access to an initial probability distribution described by a prior. Some attempts have been made to define 'objective' priors using, for instance, the maximum entropy principle. According to this principle, the most objective, or 'informationless' prior distribution is the one which maximize uncertainty. However, when data are prolific, the results coming from a Bayesian analysis are known to be insensitive to the particular choice of the prior.

The Bayesian inference scheme therefore appears as a sound and logical way for updating knowledge. Where difficulties appear is in the reliable estimations of experimental uncertainties. It is not so rare to find two or more *inconsistent* data sets, i.e., with non-overlapping error bars. Even in the case of consistent data, different evaluations of the experimental uncertainties can strongly affect the outcome of a Bayesian analysis. Most divergences between existing data libraries seem to arise purely from this bare fact.

We will not extend further this mathematical discussion here, and prefer to orient the reader toward already existing good literature on the subject- see for instance [61] and [62]. Such a Bayesian approach has been implemented in the numerical code GLUCS, "a Generalized Least-Squares Program for Updating Cross-Section Evaluations with Correlated Data Sets", developed by D.M. Hetrick and C.Y. Fu from OakRidge National Laboratory [63]. We used this particular code for the present evaluation. For details on the coding, please refer to the GLUCS user manual [63].

5.2 Example: Evaluation of ^{239}Pu (n,f)

The ^{239}Pu isotope is very abundant in the US nuclear spent fuel stream, and is therefore of primary importance in the US ATW program. Because of its importance in many applications, many experiments have been conducted to study in particular its neutron-induced fission reaction, especially below 20 MeV.

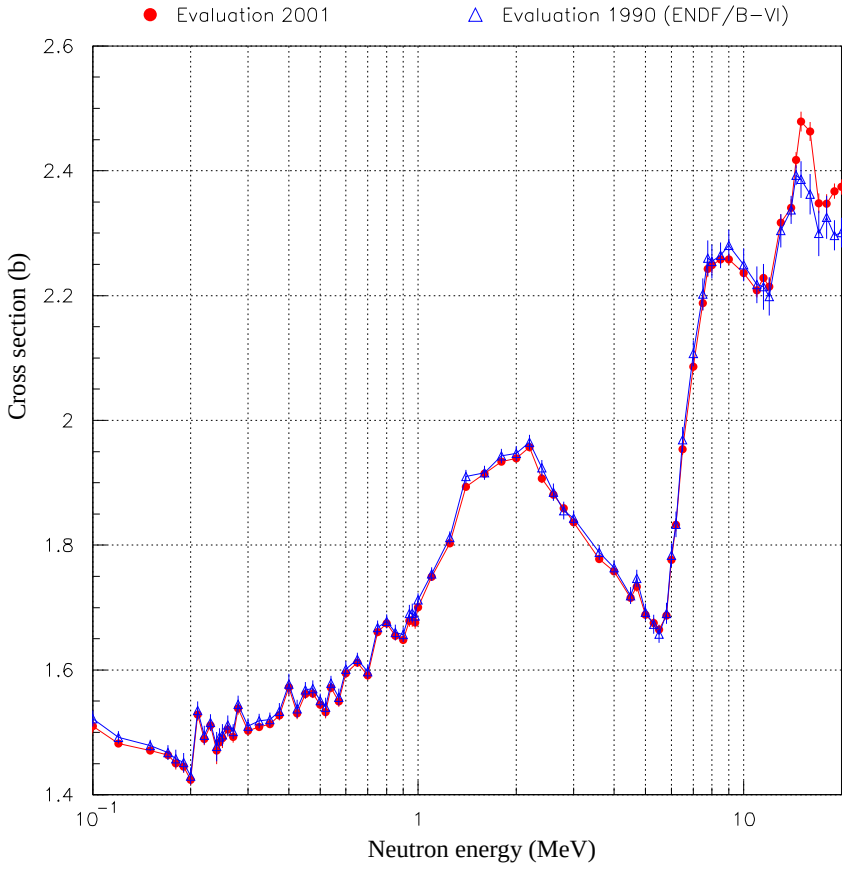

Figure 22: New ^{239}Pu (n,f) evaluation for incident neutrons energies between 0.1 and 20 MeV. This new evaluation is compared to the current ENDF/B-VI evaluation.

The set of experimental data we used differs in several respects from the one previously

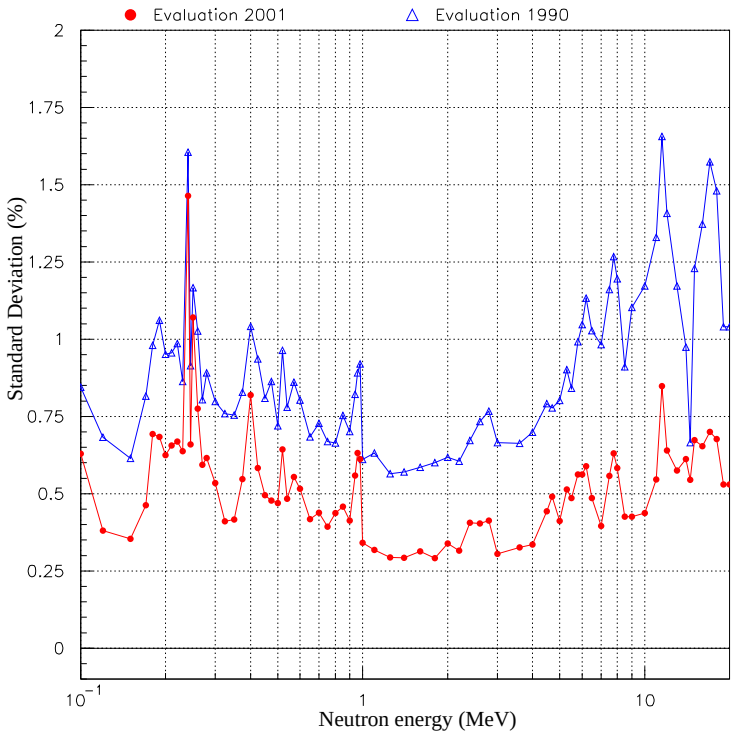

Figure 23: Standard deviations associated with the two evaluations plotted in Fig. 22.

used in the ENDF/B-VI evaluation. First, not all of the data sets used previously were included. Indeed, some relatively older experiments exhibit large uncertainties in the cross sections. While such results could be included carefully when data is scarce, the present amount of available data allows one to safely neglect them. On the other hand, several new data sets have been included in the new version. These data come from either recent experiments performed later than 1990, or data which were not present in the EXFOR database[9] by the time the last ENDF evaluation was performed; this especially concerns data from Russia. Our complete database can be found in Ref. [60].

Our new ^{239}Pu (n,f) evaluation is plotted in Fig. 22 for incident neutron energies between 0.1 and 20 MeV, along with the current ENDF/B-VI evaluation.

As can easily be seen on this figure, the two evaluations seem to be quite similar up to incident neutron energies of 14 MeV. Above this energy, the cross sections can differ by up to 4% in places. It is also interesting to note the standard deviations associated with these two evaluations. They are plotted in Fig. 23. The errors evaluated in the new evaluation appear much lower than in the previous evaluations. This is a remarkable effect of the inference process: the more knowledge we acquire on a given quantity by successive measurements, the

[9]The EXFOR database gathers experimental data set from nuclear physics experiments performed all over the World. It is maintained in different Nuclear Data Centers like the one of the IAEA, Vienna, Austria (http://iaeand.iaea.or.at/).

smaller the final uncertainties are. This phenomenon is very well illustrated in this Figure. A word of caution, though: above 14 MeV, the errors quoted in the previous evaluation were well below 2%. But we said earlier that the two evaluations could differ by as much as 4% in places! Is there not any inconsistency here? In fact, there is!

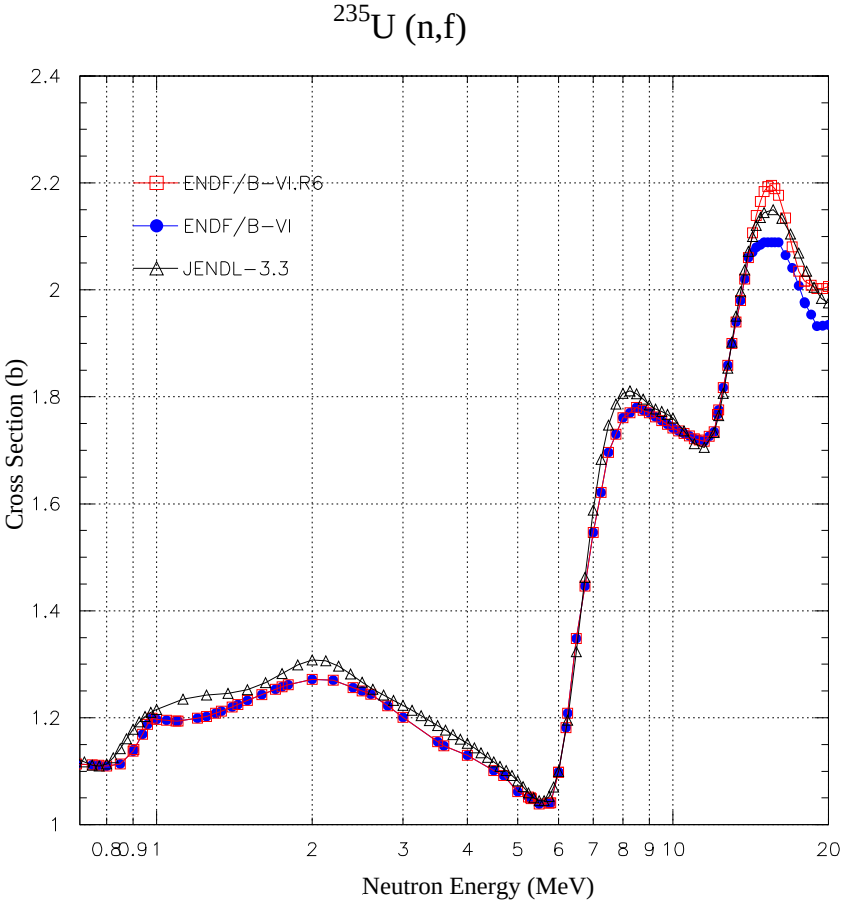

Figure 24: ^{235}U (n,f) evaluations from different libraries. The ENDF/B-VI.R6 evaluation (squares) is a recent revision of the ENDF/B-VI evaluation above 14 MeV, taking into account data from P. Lisowski [64].

The bulk of the changes of the ^{239}Pu cross section above 14 MeV are due to the revision of the *standard*[10] ^{235}U (n,f) cross section, as can be seen in Fig. 24. Obviously, the errors quoted earlier for the ^{235}U evaluation were underestimated. Therefore, the final errors on the plutonium evaluation were also largely underestimated. This should warn us about a real danger in the data evaluation process: while the mathematical tools, expressed in part by the Bayes' theorem, are well established, the greatest difficulties appear while trying to estimate correctly the experimental uncertainties. It is rather frequent to find two or more sets of experimental data *inconsistent* in the statistical sense. Obviously, at least one of the them (perhaps all!) is underestimating its uncertainties. Which one is not necessarily an

[10] A "standard" evaluation is very important as it is used as a reference for many other avaluations.

easy question...

In Fig. 25 are plotted the two most recent data sets available for the cross section ratio of ^{239}Pu (n,f) / ^{235}U (n,f), by P. Staples [65] and O. Shcherbakov [66].

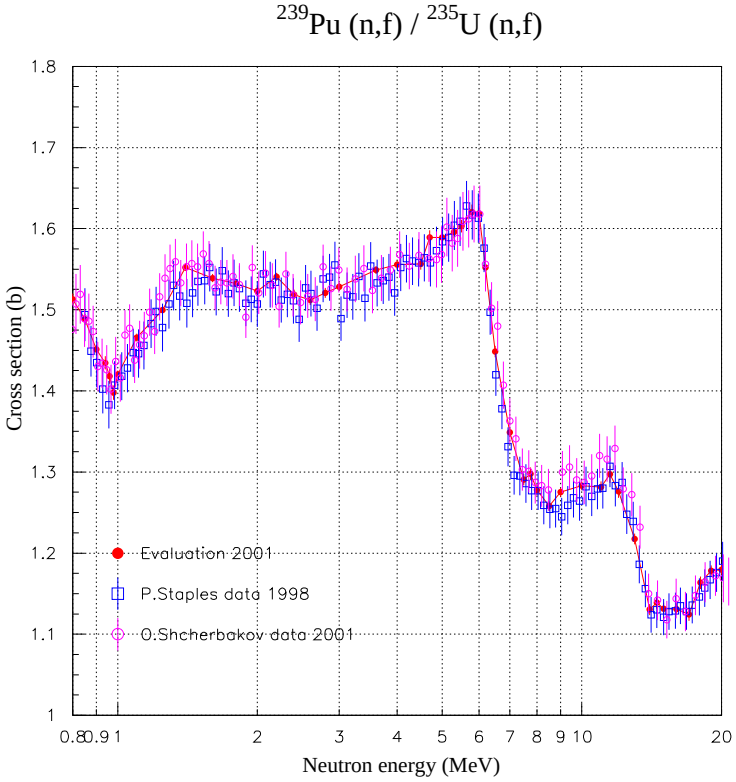

Figure 25: Evaluation of the ratio cross section ^{239}Pu (n,f) / ^{235}U (n,f), along with the two most recent experimental data sets from P.Staples et al. [65] and O.Shcherbakov et al. [66].

Finally, the Fig. 26 is very instructive: it depicts the two US ENDF evaluations (including the present one) versus the most recent JENDL one (Japanese evaluation). Large discrepancies appear in places, in particular in the 1-2 MeV energy region. In blue is plotted the ENDF evaluation obtained by using the ^{235}U (n,f) evaluation from JENDL in order to perform the transformation ratio-to-absolute evaluation. As one can see easily, a large fraction of the difference between the JENDL and ENDF ^{239}Pu (n,f) evaluations come from differences in the standard ^{235}U chosen. So far, no integral experiment has been able to clearly indicate one better evaluation.

As a concluding remark regarding the Bayesian inference scheme, we should again stress that the mathematical background is sound, while the greatest difficulties remain in the physical intuition that we have on a particular experiment and quantity. We would also like to point out two very interesting papers by K. Mosegaard and A. Tarantola [67], and by G. D'Agostini [68], both treating in detail the question of probabilistic treatments of "inverse problems".

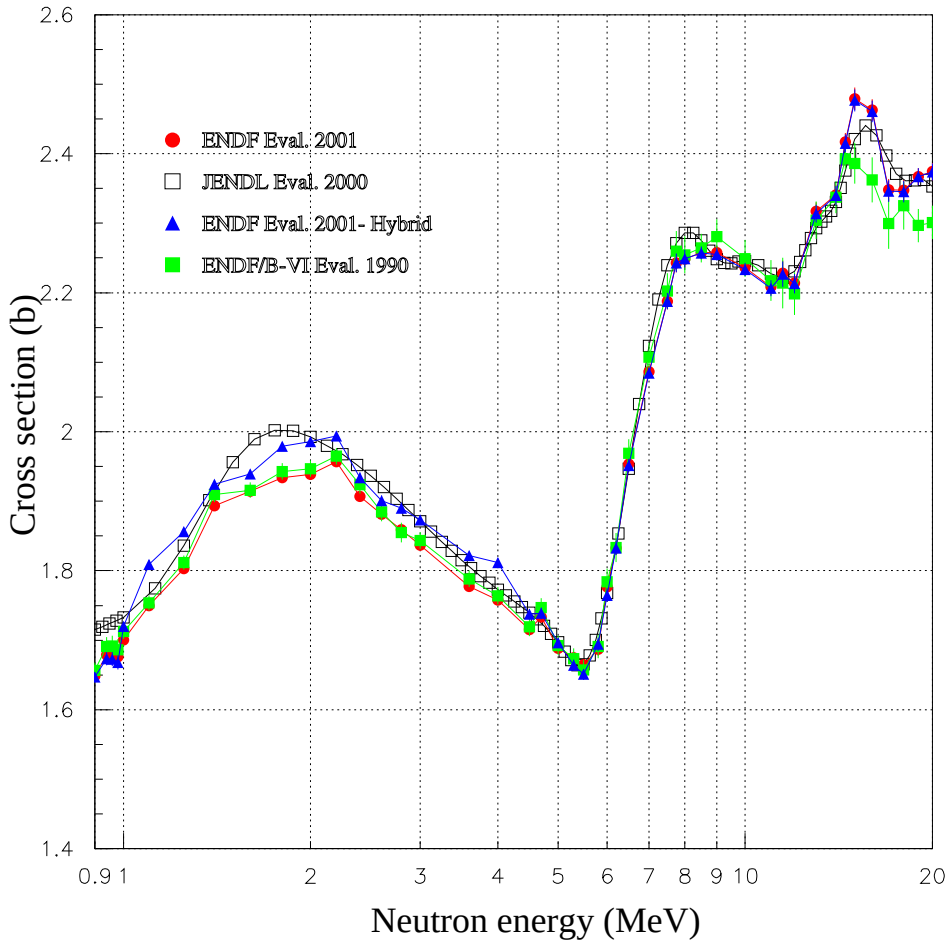

Figure 26: Comparison of several existing evaluations of ^{239}Pu (n,f).

6 Summary

Recent breakthroughs in particle accelerator technology have opened new exciting windows on basic research as well as civil applications in nuclear science and technology. Among them, one may envision for the first time the possibility of getting rid of the nagging problem of highly toxic radioactive waste by transmuting some dangerous isotopes into more stable and safer ones.

Nuclear data libraries are an important tool in the efficient and safe design of an accelerator-driven transmuter, as they allow us to predict accurately the overall behaviour of such a system. Until recently, traditional nuclear applications have driven the development of these data libraries up to the artificial energy limit of 20 MeV. On the other hand, the new ADS designs require the development of data libraries up to about 150 MeV incident neutron energies. A first and important step toward this goal has been achieved with the recent release of the neutron and proton LA150 library, covering a wide range of isotopes of interest for ADS. This library constitutes a significant improvement from earlier works, and largely contributes to the important international efforts devoted to ADS and the problem of nuclear waste.

Acknowledgments

The authors would like to thank the organizers for their kind invitation to this workshop dedicated to the challenging and important problem of nuclear waste incineration.

References

[1] Official web site of the Advanced Accelerator Applications team at Los Alamos National Laboratory: http://aaa.lanl.gov/

[2] PS Division Annual Report 2000, B.W. Allardyce, Ed., CERN/PS 2001-005 (DR); Official web site of CERN: http://welcome.cern.ch/welcome/gateway.html

[3] F. Käppeler, K.-K. Thielemann, M. Wiescher, *Current Quests in Nuclear Astrophysics and Experimental Approaches*, Annu. Rev. Nucl. Part. Sci. **48**, 175-251 (1998).

[4] M.B. Chadwick et al., Rad. Protection Dos. **170**, 1 (1997).

[5] *A Roadmap for Developing Accelerator Transmutation of Waste (ATW) Technology: a Report to Congress*, DOE, USA (1999).

[6] J.-P. Revol, *An Accelerator-Driven System for the Destruction of Nuclear Waste*, Prog. in Nucl. Energy **38**, # 1-2, 153 (2001).

[7] C. Rubbia et al., *Conceptual Design of a Fast Neutron Operated High-Power Energy Amplifier*, CERN/AT/95-44 (ET), Sept. 29, 1995; see also C. Rubbia, "A High Gain Energy Amplifier Operated with Fast Neutrons", AIP Conf. Proc. 346, Int. Conf. on ADT Technologies and Applications, Las Vegas, 1994.

[8] *The TARC Experiment (PS211): Neutron-Driven Nuclear Transmutation by Adiabatic Resonance Crossing*, CERN Yellow Report 99-11, Ed. J.-P. Revol, Dec. 1999.

[9] *A European Roadmap for Developing Accelerator Driven Systems (ADS) for Nuclear Waste Incineration*, NEA, ISBN 88-8286-008-6 (2001).

[10] T. Mukaiyama, *Review of Research and Development of Accelerator-Driven System in Japan for Transmutation of Long-Lived Nuclides*, Progress in Nuclear Energy, Vo. 38, No. 1-2, pp. 107-134 (2001).

[11] C.D. Bowman, *Accelerator-Driven Systems for Nuclear Waste Transmutation*, Annu. Rev. Nucl. Part. Sci. **48**, 505 (1998).

[12] P.G. Young, W.B. Wilson, and M.B. Chadwick, *Nuclear Data Requirements for Accelerator-Driven Transmutation Systems*, Int. Conf. on Accelerator-Driven Transmutation Technologies and Applications, July 25-29, 1994, Las Vegas, NV, USA.

[13] *Present Status of Minor Actinide Data*, NEA/OECD report, WPEC Vol. 8 (1999).

[14] V.N. Koscheev, G.N. Manturov, M.N. Nikolaev, A.M. Tsiboulia, S.M. Bedniakov, V.A. Dulin, Yu.S. Khomiakov, *Nuclear Data for Plutonium and Minor Actinides*, Proc. 3rd Int. Conf. on ADTTA, Praha, 7-11 June 1999.

[15] R.A. Forrest and J. Kopecky, *The European Activation File: EAF-2001 Cross Section Library*, EASY Documentation Series, UKAEA-FUS-451, 2001.

[16] HINDAS...

[17] *Proposal for a neutron time of flight facility: European collaboration for high-resolution measurements of neutron cross sections between 1 eV and 250 MeV.*, CERN-SPSC 99-8, SPSC/P 310, March 1999.

[18] B. Carlson, *Overview of Nuclear Reaction Theory*, this workshop.

[19] M. Herman, *Statistical Model of Nuclear Reactions- the Code Empire*, this workshop.

[20] N. Bohr, Nature **137**, 344 (1936).

[21] V.F. Weisskopf and D.H. Ewing, Phys. Rev. **57**, 472 (1940).

[22] W. Hauser and H. Feshbach, Phys. Rev. **87**, 366 (1952).

[23] P.G. Young, E.D. Arthur, and M.B. Chadwick, *Comprehensive Nuclear Model Calculations: Theory and Use of the GNASH Code*, LANL report LA-UR-96-3739, and Proc. of the workshop "Nuclear Reaction Data and Nuclear Reactors- Physics, Design, and Safety- Vol. 1", ICTP, Trieste, Italy, 15 April - 17 May, 1996, Ed. A. Gandini and G. Reffo (World Scientific, Singapore, 1999) pp 227-404.

[24] J. Raynal, *Optical Model and Coupled-Channel Calculations in Nuclear Physics*, International Atomic Energy Agency report IAEA SMR-9/8, p.281 (1970).

[25] D.G. Madland, *Recent Results in the Development of a Global Medium-Energy Nucleon-Nucleus Optical Model Potential*, Proc. Specialists Meeting on Preequilibrium Reactions, Austria, 1988, NEANDC-245, p. 103, B. Strohmaier, Ed., OECD/NEA, Paris, France (1988).

[26] M. Blann, H. Gruppelaar, P. Nagel, and J. Rodens, *International Code Comparison for Intermediate Nuclear Energy Data*, p. 1, Organization for Economic Cooperation and Development, Nuclear Energy Agency, Paris, France (1994).

[27] O. Bersillon, *SCAT2- A Spherical Optical Model Code*, Progress Report of the Nuclear Physics Division, Bruyères-Le-Châtel 1977, CEA-N-2037, p.111 (1978).

[28] A. Gilbert and G.W. Cameron, *A Composite Nuclear-Level Density Formula with Shell Corrections*, Can. J. Phys. **43**, 1446 (1965).

[29] W. Dilg, W. Schantl, H. Vonach, and M. Uhl, *Level Density Parameters for the Back-shifted Fermi Gas Model in the Mass Range 40< A < 250*, Nucl. Phys. **A217**, 269 (1973).

[30] A.V. Ignatyuk, G.N. Smirenkin, and A.S. Tishin, *Phenomenological Description of the Energy Dependence of the Level Density Parameter*, Sov. J. Nucl. Phys. **21**, 255 (1975).

[31] C. Kalbach, Phys. Rev. C **37**, 2350 (1988).

[32] H. Feshbach, A. Kerman, and S. Koonin, Ann. Phys. **125**, 429 (1980).

[33] M.B. Chadwick and P.G. Young, Phys. Rev. C **47**, 2255 (1993).

[34] M. Blann and A. Ewart, Phys. Rev. **170**, 1131 (1965).

[35] M.B. Chadwick, P.G. Young, R.E. McFarlane, and A.J. Koning, *Evaluated Nuclear Data Libraries up to 150 MeV: Method for Calculating Recoils*, Proc. 2nd Int. Conf. Accelerator-Driven Transmutation Technologies and Applications, Kalmar, Sweden, June 3-7, 1996, p. 483, H.Condé, Ed., Gotab, Stockholm, Sweden (1997).

[36] P.W. Lisowski, G.F. Auchampaugh, M.S. Moore, G.L. Morgan, and R.E. Shamu, Proc. Symp. Neutron Cross Sections from 10 to 50 MeV, Upton, New York, May 12-14, 1980, BNL-NSC-51245, p.301, Brookhaven National Laboratory (1980).

[37] R.W. Finlay, W.P. Abfalterer, G. Fink, E. Montei, T. Adami, P.W. Lisowski, G.L. Morgan, and R.C. Haight, Phys. Rev. C **47**, 237 (1993).

[38] M.B. Chadwick, P.G. Young, S. Chiba, S.C. Frankle, G.M. Hale, H.G. Hughes, A.J. Koning, R.C. Little, R.E. MacFarlane, R.E. Prael, and L.S. Waters, *Cross-Section Evaluations to 150 MeV for Accelerator-Driven Systems and Implementation in MCNPX*, Nucl. Sci. Eng. **131**, 293 (1999).

[39] A.J. Koning, J.-P. Delaroche, and O. Bersillon, *Nuclear Data for Accelerator-Driven Systems: Nuclear Models, Experiments and Data Libraries*, Nucl. Inst. Meth. **A414**, 49 (1998).

[40] M.B. Chadwick, H.G. Hughes, R.C. Little, E.J. Pitcher, and P.G. Young, *Nuclear Data for Accelerator-Driven Systems*, Prog. in Nucl. Energy **38**, # 1-2, 179 (2001).

[41] R.E. Shamu and P.G. Young, J. Phys. G **19**, L169 (1993).

[42] W.T. Wagner, G.M. Crawley, G.R. Hammerstein, and H. McManus, Phys. Rev. C **11**, 486 (1975).

[43] W.T. Wagner, G.M. Crawley, and G.R. Hammerstein, Phys. Rev. C **12**, 757 (1975).

[44] E.L. Hjort, F.P. Brady, J.R. Drummond, B. McEachern, J.H. Osborne, J.L. Romero, D.S. Sorenson, and H.H.K. Tang, Phys. Rev. C **53**, 237 (1996).

[45] V. McLane, CSISRS experimental nuclear data file, National Nuclear Data Center, Brookhaven National Laboratory (1997), http://www.nndc.bnl.gov/.

[46] M.M. Meier, D.A. Clark, C.A. Goulding, J.B. McClelland, G.L. Morgan, C.E. Moss, and W.B. Amian, *Differential neutron production cross sections and neutron yields from stoppling-length targets for 113 MeV protons*, Nucl. Sci. Eng. **102**, 310 (1989).

[47] F.S. Dietrich, W.P. Abfalterer, R.C. Haight, G.L. Morgan, F.B. Bateman, and R.W. Finlay, *Recent Measurements of Neutron Total Cross Sections on a Wide Range of Targets from 5 to 600 MeV at LANSCE/WNR*, Proc. Int. Conf. Nuclear Data for Science and Technology, Trieste, Italy, May 19-24, 1997, p.402, G. Reffo, Ed. ENEA, Bologna, Italy (1997).

[48] P. Kirby and W.T. Link, Can. J. Phys. **44**, 1847 (1966).

[49] A. Marcinkowski, R.W. Finlay, J. Rapaport, P.E. Hodgson, and M.B. Chadwick, Nucl. Phys. **A501**, 1 (1989).

[50] R.C. Haight, F.B. Bateman, S.M. Sterbenz, M.B. Chadwick, P.G. Young, S.M. Grimes, O.A. Wasson, P. Maier-Komor, and H. Vonach, *The $^{58,60}Ni$ (x, α) reactions from threshold to 50 MeV*, Proc. Int. Conf. Nuclear Data for Science and Technology, Trieste, Italy, May 19-24, 1997, p.603, G. Reffo, Ed., ENEA, Bologna, Italy (1997).

[51] J.R. Wu, C.C. Chang, and H.D. Holmgren, Phys. Rev. C **19**, 698 (1979).

[52] A.M. Kalend, B.D. Anderson, A.R. Baldwin, R. Madey, J.W. Watson, C.C. Chang, H.D. Holmgren, R.W. Koontz, J.R. Wu, and H. Machner, Phys. Rev. C **28**, 105 (1983).

[53] F.E. Bertrand and R.W. Peelle, Phys. Rev. **8**, 1045 (1973).

[54] R. Michel and P. Nagel, "International Codes and Model Intercomparison for Intermediate Energy Activation Yields", NSC/DOC(97)-1, p. 1, OECD/NEA, Paris, France (1997).

[55] Hughes et al., *MCNPX for neutron-proton transport*, Aragones, J.M., Ed., Proc. of the Mathematics and Computation, Reactor Physics and Environmental Analysis in Nuclear Applications. (Spain: Senda Editorial, S.A., Madrid), Madrid, Spain, September 27-30, 1999.

[56] T. Nakamura, M. Fujii, and K. Shin, *Neutron production from thick targets of carbon, iron, copper and lead by 30 and 52 MeV protons*, Nucl. Sci. Eng. **83**, 444 (1982).

[57] R.E. MacFarlane and D.W. Muir, *The NJOY Nuclear Data Processing System, Version 91*, Tech. Rept. LA-12740-M (1994). Los Alamos National Laboratory, Los Alamos, NM.

[58] M.B. Chadwick, H.H. Barschall, R.S. Caswell, P.M. DeLuca, G.M. Hale, D.T.L. Jones, R.E. MacFarlane, J.P. Meulders, H. Schuhmacher, U.J. Schrewe, A. Wambersie, and P.G. Young, *A consistent set of neutron kerma coefficients from thermal to 150 MeV for biologically important materials*, Med. Phys. **26**, 974 (1999).

[59] H. Poincaré, "Science and Hypothesis", 1905 (Dover publications, 1952).

[60] P. Talou, P.G. Young, and M.B. Chadwick, *Improved Evaluation of ^{239}Pu (n,f) between 0.1 and 20 MeV Incident Neutrons Energies*, Proc. of the Conf. on "Nuclear Applications in the New Millenium", Reno, NV, Nov. 11-15, 2001.

[61] D.L. Smith, *Probability, Statistics, and Data Uncertainties in Nuclear Science and Technology*, OECD/NEA Nuclear Data Committee Series on "Neutron Physics and Nuclear Data in Science and Technology", Vol. 4 (1991).

[62] F.H. Fröhner, *Evaluation and Analysis of Nuclear Resonance Data*, OECD/NEA JEFF Report 18 (2000).

[63] D.M. Hetrick and C.Y. Fu, "GLUCS: A Generalized Least-Squares Program for Updating Cross Section Evaluations with Correlated Data Sets", ORNL/TM-7341, ENDF-303, 1980.

[64] P.G. Young and M.B. Chadwick, 1998 (unpublished).

[65] P. Staples and K. Morley, Nuclear Science and Engineering **129**, 149-163 (1998).

[66] O. Scherbakov et al., ISTC 609-97, 2001 (and private communication).

[67] K. Mosegaard and A. Tarantola, *Probabilistic Approach to Inverse Problems*, International Handbook of Earthquake and Engineering Seismology, Academic Press for the International Association of Seismology and Physics of the Earth Interior- IASPEI (2001).

[68] G. D'Agostini, *Bayesian Reasoning in High Energy Physics - Principles and Applications* -, CERN Yellow Report 99-03 (1999).